Marine Chemistry xxx (xxxx) xxx–xxx

Contents lists available at ScienceDirect

Marine Chemistry

journal homepage: www.elsevier.com/locate/marchem

The Carbon:^{234}Thorium ratios of sinking particles in the California current ecosystem 1: relationships with plankton ecosystem dynamics

Michael R. Stukel[a,b,*], Thomas B. Kelly[a], Lihini I. Aluwihare[c], Katherine A. Barbeau[c], Ralf Goericke[c], Jeffrey W. Krause[d], Michael R. Landry[c], Mark D. Ohman[c]

[a] Dept. of Earth, Ocean, and Atmospheric Science, Florida State University, Tallahassee, FL, United States
[b] Center for Ocean-Atmospheric Prediction Studies, Florida State University, Tallahassee, FL, United States
[c] Scripps Institution of Oceanography, University of California San Diego, San Diego, CA, United States
[d] Dauphin Island Sea Lab, University of South Alabama, Dauphin Island, AL, United States

A B S T R A C T

We investigated variability in the C:^{234}Th ratio of sinking particles and its relationship to changing water column characteristics and plankton ecological dynamics during 29 Lagrangian experiments conducted on six cruises of the California Current Ecosystem Long-Term Ecological Research (CCE-LTER) Program. C:^{234}Th ratios of sinking particles collected by a surface-tethered sediment trap (C:$^{234}Th_{ST}$) varied from 2.3 to 20.5 μmol C dpm^{-1} over a depth range of 47–150 m. C:$^{234}Th_{ST}$ was significantly greater (by a factor of 1.8) than C:^{234}Th ratios of suspended > 51-μm particles collected in the same water parcels with *in situ* pumps. C:^{234}Th ratios of large (> 200-μm) sinking particles also exceeded those of smaller sinking particles. C:$^{234}Th_{ST}$ decreased with depth from the base of the euphotic zone through the upper twilight zone. C:$^{234}Th_{ST}$ was positively correlated with several indices of ecosystem productivity including particulate organic carbon (POC) and chlorophyll (Chl) concentrations, mesozooplankton biomass, and the fraction of Chl > 20-μm. Principal component analysis and multiple linear regression suggested that decaying phytoplankton blooms exhibited higher C:$^{234}Th_{ST}$ than actively growing blooms at similar biomass levels. C:$^{234}Th_{ST}$ was positively correlated with indices of the fractional contribution of fecal pellets in sediment traps when the proportion of fecal pellets was low in the traps, likely because of a correlation between mesozooplankton biomass and other indices of ecosystem productivity. However, when fecal pellets were a more important component of sinking material, C:$^{234}Th_{ST}$ decreased with increasing fecal pellet content. C:$^{234}Th_{ST}$ was also positively correlated with the Si:C ratio of sinking particles. Across the dataset (and across depths) a strong correlation was found between C:$^{234}Th_{ST}$ and the ratio of vertically-integrated POC to vertically-integrated total water column ^{234}Th (^{v}C:$^{234}Th_{tot}$). A mechanistic one-layer, two-box model of thorium sorption and desorption was invoked to explain this correlation. Two empirical models (one using ^{v}C:$^{234}Th_{tot}$; one using depth and vertically-integrated Chl) were developed to predict C:^{234}Th ratios in this coastal upwelling biome. The former regression ($\log_{10}$(C:$^{234}Th_{ST}$) = 0.43 × $\log_{10}$(^{v}C:$^{234}Th_{tot}$) + 0.53) was found to also be a reasonable predictor for C:$^{234}Th_{ST}$ from diverse regions including the Southern Ocean, Sargasso Sea, Subarctic North Pacific, and Eastern Tropical North Pacific.

1. Introduction

The biological carbon pump (BCP) refers to a suite of processes that transport organic carbon produced in the euphotic zone into the deep ocean, leading to a net removal of carbon dioxide from the atmosphere (Buesseler and Boyd, 2009; Ducklow et al., 2001; Volk and Hoffert, 1985). In most oceanic regions, it is assumed that the BCP is dominated by the flux of sinking particles (including marine snow, phytodetritus, and zooplankton fecal pellets). Current estimates of the global magnitude of the BCP range from 5 to 13 Pg C yr^{-1} (Dunne et al., 2005; Henson et al., 2011; Laws et al., 2011; Siegel et al., 2014). This large uncertainty contributes to difficulties in predicting changes in the BCP under future climate scenarios.

While early measurements of sinking carbon export from the

Abbreviations: CCE, California Current Ecosystem; dpm, decays per minute = 1/60 Bq; BCP, Biological carbon pump; ^{v}C:$^{234}Th_{tot}$, vertically-integrated POC/vertically-integrated total water column ^{234}Th

* Corresponding author.
E-mail address: mstukel@fsu.edu (M.R. Stukel).

https://doi.org/10.1016/j.marchem.2019.01.003
Received 17 October 2018; Received in revised form 15 January 2019; Accepted 15 January 2019

euphotic zone were primarily made with sediment traps, the past two decades have seen a rapid increase in the use of radionuclide disequilibrium techniques for measuring particle flux. ^{238}U:^{234}Th disequilibrium, in particular, has been extensively used as a result of: 1) the development of relatively simple analytical methods and 2) a measurement time scale (~1 month) that corresponds well with changes in pelagic communities (Le Moigne et al., 2013; Van der Loeff et al., 2006; Waples et al., 2006). This methodological approach works because, while ^{238}U is nearly conservative in the water column and covaries with salinity (Chen et al., 1986; Owens et al., 2011), its daughter nuclide (^{234}Th) exists in seawater in the particle-reactive Th(IV) oxidation state, which gets removed from the surface ocean when particles sink to depth (Buesseler et al., 1992; Coale and Bruland, 1985; Santschi et al., 2006). This leads to a deficit of ^{234}Th relative to secular equilibrium with ^{238}U that can be converted into ^{234}Th flux estimates by either time-series measurements of ^{234}Th or (more commonly) a steady state assumption (Savoye et al., 2006). This approach thus allows efficient and rapid quantification of carbon flux without repeated or prolonged station occupations (as are necessary with sediment trap measurements). However, the ^{234}Th approach requires that a C:^{234}Th ratio be estimated to convert Th flux to C flux (Buesseler et al., 2006).

Conceptually, the C:^{234}Th ratio should be measured on material that is representative of the average particles exported across the depth horizon of interest during the period of time over which the ^{234}Th disequilibrium approach integrates (*i.e.* ~30 d). However, many approaches exist for collecting putatively sinking particles (McDonnell et al., 2015), and the technique used varies greatly based on the sampling plan employed on a particular cruise. Although the ideal approach would be to use sediment traps that have been tested to ensure relatively minimal collection bias, such deployments are time consuming and often inconsistent with taking ^{234}Th measurements on transects or other Eulerian sampling schemes. Instead, many studies rely on the collection of large particles (*e.g.* > 50-μm) by large volume *in situ* pumps deployed at depth (*e.g.*Black et al., 2017; Owens et al., 2015). This approach meshes well with typical sampling plans, because at shallow depths sufficient particles can often be collected in 1–4 h. However, sinking speed is not always tied to particle size and < 64-μm particles have been shown to be a quantitatively important portion of total particle flux (Durkin et al., 2015; Hung et al., 2012; McDonnell and Buesseler, 2010). Furthermore, simultaneous collection of particles by sediment traps and *in situ* pumps have shown significant differences in measured C:^{234}Th ratios (Buesseler et al., 2009; Hung et al., 2010; Lepore et al., 2009; Murray et al., 1996; Stewart et al., 2007; Stukel et al., 2016).

In situ particulate C:^{234}Th ratios are controlled by a suite of processes that prevent *a priori* estimation of C:^{234}Th ratios (Buesseler et al., 2006; Burd et al., 2007; Passow et al., 2006; Santschi et al., 2006; Savoye et al., 2006). Since thorium is adsorbed onto particle surfaces while C increases roughly linearly with particle volume, the C:^{234}Th ratio might be expected to increase with increasing particle size. However, if sinking marine snow is formed by the aggregation of smaller particles, no size dependency of C:^{234}Th may be evident. Alternatively, when microbial remineralization causes particles to decrease in size as they sink, we should expect preferential remineralization of carbon to lead to reduced C:^{234}Th with decreasing particle size (Buesseler et al., 2006). This same process may lead to changing C:^{234}Th ratios with depth, although similar decreases of C:^{234}Th ratios with depth may be caused by the aforementioned mechanism or by continued adsorption combined with increased total ^{234}Th activity at depth. C:^{234}Th may also be controlled by particle type, with fecal pellets potentially enriched in C:^{234}Th relative to phytoplankton (if zooplankton do not assimilate Th) and zooplankton carcasses depleted in Th. The abundance of sticky acid polysaccharides (including those contained in transparent exopolymeric particles, TEP) can also alter C:^{234}Th ratios as Th readily binds to sorption sites on these molecules (Guo et al., 2002; Passow et al., 2006; Quigley et al., 2002; Zhang et al., 2008), although the impact of these polysaccharides on the C:^{234}Th ratio of sinking particles will depend on whether they are aggregated into the sinking particle fraction or remain suspended in the surface waters. Indeed, Th can at times be complexed primarily to colloidal acid polysaccharides and humic acids, suggesting that the ratio of colloidal and dissolved organic carbon (DOC) to POC may impact C:^{234}Th ratios on sinking particles (Murphy et al., 1999).

Clearly a better understanding of the processes driving variability in C:^{234}Th ratios would benefit studies in which sinking particles are sampled with much less frequency than water column ^{234}Th (*e.g.*Ducklow et al., 2018; Estapa et al., 2015; Puigcorbé et al., 2017; van der Loeff et al., 2011) and aid in the parameterization of biogeochemical models that explicitly include ^{234}Th as a state variable (Resplandy et al., 2012). In this study we use results from 29 Lagrangian experiments conducted in the southern California Current Ecosystem (CCE) to investigate the variability of the C:^{234}Th ratio of sinking particles and its relation to biogeochemical (*e.g.* POC and nutrient concentrations, carbon flux) and ecological (*e.g.* primary productivity, mesozooplankton biomass and grazing, phytoplankton abundance, size distributions, and taxonomic compositions) parameters. The southern CCE is a useful study site, because it is a region with extensive spatiotemporal variability in physical drivers, system productivity, and plankton community composition (Goericke, 2011; Goericke and Ohman, 2015; Ohman et al., 2013). Our goal in this study is not to conduct detailed experiments designed to elucidate mechanisms controlling Th speciation, but rather to investigate patterns relating *in situ* C:^{234}Th ratios to potential ecosystem drivers. In a companion manuscript, we compare *in situ* C:^{234}Th ratios to a mechanistic model that combines a discrete particle formation and sinking model with a ^{234}Th sorption, desorption, and decay model (Stukel and Kelly, this issue).

2. Methods

2.1. Lagrangian sampling scheme

Samples for this study were collected on six Process cruises of the CCE Long-Term Ecological Research (LTER) Program (Fig. 1). On each cruise sampling plans featured multiple two- to five-day quasi-Lagrangian experiments (referred to as “cycles”) that allowed extended sampling of biogeochemical and ecological rates and standing stocks during the short-term evolution of a water parcel. Results from a total of 29 cycles are included in this study. Prior to each cycle we used satellite remote sensing products and a Moving Vessel Profiler (MVP, Ohman et al., 2012) to survey regions of interest. Cycles were initiated with the deployment of a sediment trap with attached 3 × 1-m holey sock

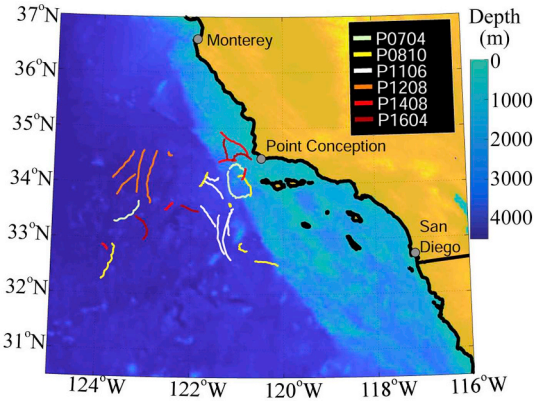

Fig. 1. Location of quasi-Lagrangian cycles and bathymetry of study region. Tracks are colored according to cruise. P0704 = April 2007, P0810 = October 2008, P1106 = June 2011, P1208 = August 2012, P1408 = August 2014, P1604 = April 2016.

drogue centered at 15-m to track mixed layer communities (Stukel et al., 2013). Following sediment trap deployment a CTD-Niskin rosette cast was conducted to collect water for *in situ* experiments conducted at 6–8 depths spanning the euphotic zone (^{14}C-primary productivity, microzooplankton grazing dilution experiments, $^{15}NO_3^-$ uptake). Bottles were incubated *in situ* for 24 h on an experimental array with an identical holey sock drogue centered at 15-m depth (Landry et al., 2009). Every morning at ~04:15 the experimental array was recovered, a new set of incubations was placed on the array, and the array was redeployed, thus allowing for daily vertical profiles of each set of rate measurements. The experimental array also served as a Lagrangian frame of reference for a suite of additional measurements including: ^{234}Th:^{238}U disequilibrium (Stukel et al., 2011), mesozooplankton biomass and gut pigment-derived grazing rates (Landry et al., 2009; Ohman et al., 2012), fluorometer-determined phytoplankton pigments, nutrients, particulate organic carbon (POC), total organic carbon (TOC), flow cytometry-derived picoplankton abundance and biomass (Taylor et al., 2012), epifluorescence microscopy-derived nano- and microplankton abundance and biomass (Taylor et al., 2012), and biogenic silica (Krause et al., 2015). With the exception of mesozooplankton measurements (which utilized oblique net tows that integrated the surface ~210-m of the water column) all measurements listed above were made at 6–8 depths spanning the euphotic zone (surface to ~0.1% light level).

2.2. Water column ^{234}Th measurements

^{234}Th was measured in whole, unfiltered seawater samples using standard small volume methods (Benitez-Nelson et al., 2001; Pike et al., 2005) at 8–12 depths spanning the upper 150–200 m. 4-L samples were drawn from Niskin rosettes, immediately acidified with ~8-mL HNO_3^- to a pH < 2, and spiked with 1 mL ^{230}Th yield tracer. Samples were shaken and left to equilibrate for 4–9 h. NH_4OH was then added to modify pH to 8–9 and $KMnO_4$ and $MnCl_2$ were added to allow co-precipitation of thorium on manganese oxide. After > 8 h, samples were vacuum filtered through quartz (QMA) filters, dried, and mounted on Risø sample holder (nylon disc planchette). Samples were beta counted on a Risø GM-25-5 low-level beta multi-counter either on land (University of South Carolina) immediately following the cruise (cruises P0704, P0810, and P1106) or at sea (P1208, P1408, and P1604). Samples were background counted > 6 half-lives after initial count. For cruises P1408 and P1604, additional counts were performed between initial and background counts. Samples were then dissolved in H_2O_2/HNO_3^- solution, spiked with ^{229}Th yield tracer. Thorium was purified by column chromatography in AG1-X8 resin. Thorium filtration yield was then calculated from the $^{229:230}$Th ratio measured on a Thermo Element 2 inductively-coupled plasma mass spectrometer at the Woods Hole Oceanographic Institution Analytical Facility or at the National High Magnetic Field Laboratory. ^{238}U—^{234}Th deficiency was quantified by estimating ^{238}U from salinity using the equations in Owens et al. (2011). ^{234}Th flux was quantified from ^{238}U—^{234}Th deficiency profiles using a one-dimensional steady-state equation: ^{234}Th Export = $\lambda_{234} \times (A_{U238}\text{-}A_{Th234})$, where λ_{234} is the decay constant for ^{234}Th and A_{U238} and A_{Th234} are the vertically-integrated activities of ^{238}U and ^{234}Th, respectively (Savoye et al., 2006). Samples for analysis of the C:^{234}Th ratio were collected either using a McLane WTS-LV *in situ* pump (P0704, P0810, and P1106) and/or with a surface-tethered drifting sediment trap (all cruises, see below). *In situ* pump samples were typically collected on a 147-mm, 50-µm mesh filter and rinsed onto a QMA filter that was mounted in a Risø sample holder and analyzed as above.

2.3. Sediment trap deployments

VERTEX-style Particle Interceptor Tube (PIT) sediment traps (Knauer et al., 1979) were deployed at a depth of 100 m on all cruises and also typically at a depth slightly below the euphotic zone if the euphotic zone was shallower than 70 m. On P1408 and P1604 cruises, sediment traps were also deployed at a depth of 150 m. PITs were constructed from acrylic tubes with a 69.85-mm internal diameter and 8:1 aspect ratio and had a baffle on top comprised of thirteen 76-mm long, 12.7-mm internal diameter acrylic tubes that were carefully beveled on the top using a lathe. Typically 8–12 PIT tubes were deployed per depth on PVC cross-pieces attached to a line hanging beneath the mixed layer drogue. PITs were deployed with a saltwater brine consisting of filtered seawater amended with 50 g L^{-1} NaCl and 0.4% formaldehyde (final concentration). Immediately after recovery, the interface between brine water and overlying surface water was determined for each tube and gentle suction was utilized to remove overlying water to a height of ~3 cm above the interface. On the P1106 cruise, salinity measurements were made before and after deployment and confirmed that brine solution was minimally diluted (median 5% of final volume) by mixing with natural seawater (Krause et al., 2015). Samples were then gravity filtered through 47-mm, 202-µm filters, and swimming mesozooplankton were removed from the filters under a stereomicroscope. For most samples, the > 202-µm fraction was then rinsed back into the original sample (*i.e.* < 202- and > 202-µm fractions were combined). However, on cruises P1208, P1408, and P1604, < 202- and > 202-µm fractions were analyzed separately for size-fractionated C:^{234}Th ratios.

Tubes were then split on a Folsom splitter and used for a series of analyses. Particulate organic carbon and nitrogen (POC and PON) samples were filtered through 25-mm pre-combusted glass fiber (GF/F) filters and analyzed by either a CHN elemental analyzer or an isotope ratio mass spectrometer (for additional isotope data) at the Scripps Institution of Oceanography Analytical Lab. Samples for biogenic Si (bSi) were filtered onto 47-mm, 0.6-µm pore size polycarbonate filters and analyzed using a NaOH digestion method (Krause et al., 2015). Samples for chlorophyll and phaeopigments were filtered onto GF/F filters and analyzed by fluorometry with acidification (Strickland and Parsons, 1972). Samples for fecal pellet enumeration were stored in formaldehyde until analysis by stereomicroscopy (Morrow et al., 2018; Stukel et al., 2013). Samples for C:^{234}Th ratios were filtered through QMA filters and analyzed as above. On P0704, P0810, and P1106 cruises, whole samples were filtered for C:^{234}Th. On P1208, P1408, and P1604 cruises, the < 202-µm and > 202-µm size fractions were filtered and analyzed separately. After initial and background beta counts, QMA filters were analyzed for C and N by CHN elemental analyzer. Swimming mesozooplankton picked from a subset of the sediment trap deployments were filtered through QMA filters and analyzed as above for C:^{234}Th ratio.

2.4. Data manipulation and statistical analyses

Vertical integrations were calculated using a simple trapezoidal rule when the integration depth was shallower than the depth of the deepest samples. However, on some cycles, suspended POC concentrations were only measured to the base of the euphotic zone (not the deepest sediment trap depth). To extend these profiles deeper, we used 86 profiles for which POC was measured to deeper depths and determined that (on average) suspended POC decreased by 1.5% m^{-1} beneath the euphotic zone (standard error = 0.2%). This exponential extrapolation was used to estimate vertically integrated POC from the deepest sampling depth to the sediment trap depth. For phytoplankton related rates and standing stocks (*e.g.* primary production, Chl), we integrated only to the deepest sampling depth (which was at or slightly below the base of the euphotic zone) because we assume that phytoplankton biomass was negligible beneath the euphotic zone.

When comparing different properties (*e.g.* C:^{234}Th ratio of sinking particles to primary production), we used Type II linear regression using the methods of York et al. (2004), which incorporate variable uncertainty on different data points. Uncertainties of data points were

quantified as the standard error of multiple measurements made on the same quasi-Lagrangian cycle. Type II linear models are not intended to imply that the underlying relationship is linear, but rather to explore patterns in covariance between properties. To test for correlations between properties, we used the non-parametric Spearman's rank test in the Matlab function 'corr'. Type II linear regression models are only plotted if the Spearman's rank correlation was statistically significant ($p < .05$). Because relationships between parameters may not be linear, we also plot the relationships using a moving regression. We used locally-estimated scatterplot smoothing (LOESS) implemented with the fLOESS function in Matlab. fLOESS employs a second degree polynomial to smooth one dimensional data. We used a span equal to half of the available measurements. Moving regressions may not necessarily capture the functional relationships between variables but are plotted to allow visual representations of the (potentially nonlinear) relationships between ecosystem properties.

2.5. Outlier analysis

To test for outliers in the C:^{234}Th ratio of sinking particles measured by sediment trap, we used the Matlab function 'isoutlier'. isoutlier identifies any point as an outlier if it is more than three scaled median absolute deviations away from the median. Two data points were determined to be outliers: Cycle P0810–1 at 50 m depth and Cycle P1408–1 at 60 m depth. P0810–1 at 50 m had a C:^{234}Th ratio of 20.5 μmol dpm^{-1} and P1408–1 at 60 m had a value of 14.8 μmol dpm^{-1}, compared to a median (across all sediment trap samples) of 6.1 μmol dpm^{-1}. These samples were investigated in further detail. Triplicate samples from P0810–1 at 50 m had values of 23.6, 20.4, and 17.7 μmol dpm^{-1} and triplicate samples from P1408–1 at 60 m had values of 14.2, 17.4, and 12.7 μmol dpm^{-1}. These high values were thus not driven by a single erroneous sample. For P0810–1 at 50 m the paired *in situ* pump sample also had the highest C:^{234}Th ratio found in the *in situ* pump dataset. We therefore conclude that these two values reflect true variability in the C:^{234}Th ratio and include them in all figures and regression analyses.

2.6. Principal component analysis and linear models

Because many water column properties co-vary (*e.g.*, primary production, Chl), we first performed principal component analysis (PCA). Our ecological data was highly skewed (*i.e.* many datasets had many values clustered at low positive values, but a long tail of high positive values). Hence, individual variables were log-transformed prior to PCA if the log-transformed data better approximated a normal distribution than the un-transformed data (as determined by a higher *p*-value of a Kolmogorov-Smirnov test with a normal distribution; Matlab function 'kstest'). This resulted in log-transformation of all variables except depth and silica excess (*i.e.* [silicic acid] – [nitrate]). Such transformation is recommended by Wold et al. (1987), because outliers can significantly impact PCA results. Without transformation, the PCA would have been driven almost entirely by patterns under high-biomass, high-nutrient bloom conditions and patterns emerging during oligotrophic conditions would have been obscured. Following log transformation all variables were then centered and scaled by subtracting off the mean and dividing by the standard deviation. Because not all variables of interest were measured on each cycle (across the dataset 11% of the data points were missing), we then filled the dataset (*i.e.*, estimated missing values) using multiple imputation by chained equations. 1000 different filled datasets were produced using the R package MICE (Buuren and Groothuis-Oudshoorn, 2010). PCA was then performed using the function 'pca' in Matlab on each of the 1000 different filled datasets. Uncertainty in the PCA was computed from the differences between PCA results for these different datasets.

We then used step-wise linear regression to investigate the dependence of sinking C:^{234}Th ratios on water column characteristics. The first three principal components were included as predictor variables as were depth and the ratio of vertically integrated POC to vertically integrated total water column ^{234}Th above the trap depth (^{v}POC:^{234}Th$_{tot}$). Step-wise linear regression (Matlab function 'stepwisefit') was performed on each of the imputed datasets to determine the variables that added predictive power to the regression and develop a best fit equation. This function begins with a model using only a y-intercept to predict the dependent variable. It then iteratively adds or subtracts potential independent variables to the model if the addition or subtraction of the independent variable adds explanatory power as determined by the *p*-value of the F-statistic. Terms are added in order of the minimum *p*-value of the F-statistic and removed from the model in order of the largest *p*-value of the F-statistic. Stepwise linear regression does not necessarily find the optimal model to explain the data and was used only for exploration of the data. Stepwise regressions were conducted on each of the imputed datasets (see above) to explore uncertainty in regression statistics.

To test the predictive power of this approach, we conducted bootstrapping analyses with datasets withheld in the following manner: A random filled dataset was chosen from the 1000 imputed datasets. Half of the data points in this dataset were then chosen at random and used to compute a multiple linear regression for each of the equations identified as statistically significant during the step-wise linear regression approach. Regressions were also computed with individual parameters. These linear regressions were then used to predict the C:^{234}Th values of the half of the datasets that had been withheld from the regression. Root mean squared error (RMSE) was used to quantify the linear model-data misfit. This bootstrapping analysis was computed for 10,000 total iterations. This approach was used to determine whether added variables increased the predictive power of equations used to predict C:^{234}Th ratios of sinking particles from biological and chemical properties measured in the euphotic zone.

3. Results

3.1. Description of water parcels

Conditions encountered on the 29 Lagrangian experiments included in this study spanned much of the natural variability in the CCE. Primary productivity varied from 9.9 to 191 mmol C m^{-2} d^{-1} and surface Chl varied from 0.07 to 4.2 μg Chl a L^{-1}. On cruises P0704 (April 2–21, 2007) and P0810 (September 30–October 29, 2008), experimental cycles were intentionally chosen to span the spatial variability found in the region during non-El Niño conditions. Consequently, variability on these cruises was large, with experiments conducted in both upwelling-influenced and highly oligotrophic waters (for additional cruise details, see Landry et al., 2012; Stukel et al., 2012). The P1408 (August 6 – September 4, 2014) and P1604 (April 19 – May 12, 2016) cruises sampled similar regions during the North Pacific warming event in 2014–2015 and the ensuing 2015–2016 El Niño (Kelly et al., 2018; Morrow et al., 2018; Nickels and Ohman, 2018). During this time, sea surface temperatures were elevated throughout the region, upwelling was restricted near the coast, and primary productivity was depressed region wide (Kahru et al., 2018). The P1106 (June 18 – July 17, 2011) and P1208 (July 28 – August 26, 2012) cruises were specifically designed to investigate the response of plankton communities to ocean fronts associated with mesoscale eddies. Hence Lagrangian experiments were conducted within and on either side of gradient regions that separated productive coastal waters from oligotrophic offshore domains (Krause et al., 2015; Stukel et al., 2017).

We used principal component analysis to investigate covariance in water column properties (Fig. 2). The first principal component separated the data based on overall biomass and productivity of the system and explained 55.4 ± 1.6% of the variability. It had strong coefficients for primary productivity, vertically-integrated POC, vertically-integrated Chl, surface POC, surface Chl, surface NO_3^-, percent Chl >

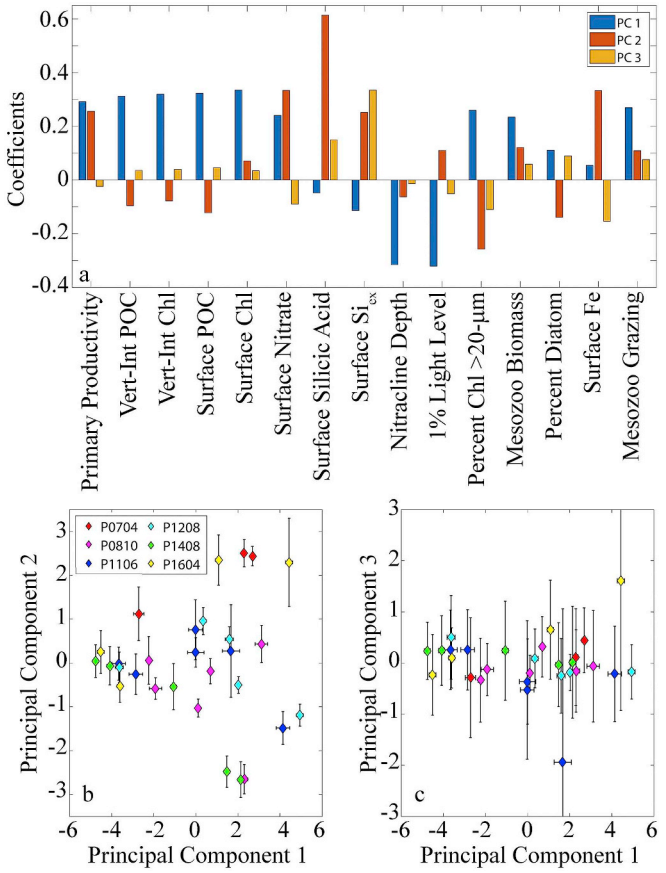

Fig. 2. Principal component analysis of water column properties. a) Coefficients for each measured parameter with each of the first three principal components. b and c) PC1 plotted against PC2 and PC3, respectively. Colors represent different cruises.

20-µm, and mesozooplankton biomass and negative coefficients for the depth of the nitracline and 1% light level. The second principal component (14.1 ± 1.0% of the variability) largely divided the dataset based on nutrient concentration and productivity. It showed near zeros coefficients for most biomass proxies, but strongly positive coefficients for primary productivity and all nutrients (NO_3^-, Si, Fe). The third principal component (10.0 ± 1.1% of the variability) was dominated by positive coefficients for surface silicic acid and silica excess and may reflect whether or not the diatom community was Fe-limited.

3.2. Variability in the C:^{234}Th ratio

Across the dataset, the C:^{234}Th ratio of sinking particles collected in sediment traps varied from 2.3 ± 0.2 µmol C dpm^{-1} to 20.5 ± 3.0 µmol C dpm^{-1} (Table 1). This approximately order of magnitude variability was notably comparable to variability in ^{234}Th export flux at the 100 m depth horizon computed using a 1-dimensional steady-state model (317 to 3369 dpm m^{-2} d^{-1}). Furthermore, C:^{234}Th ratios were correlated with steady-state ^{234}Th flux (Spearman's $\rho = 0.54$, $p = 2 \times 10^{-5}$). This suggests that using a constant C:^{234}Th ratio to quantify carbon flux from ^{234}Th flux measurements in the CCE would underestimate carbon flux variability.

C:^{234}Th ratios of large particles collected by *in situ* pump were significantly lower than C:^{234}Th ratios of sinking particles collected by sediment traps (Fig. 3a). The geometric mean of sediment trap C:^{234}Th ratios divided by C:^{234}Th ratios of *in situ* pump samples (for paired samples) was 1.81 with a 95% confidence interval (C.I., determined by non-parametric Monte Carlo error analysis) of 1.57–2.08. Large (> 200-µm) sinking material also had significantly higher C:^{234}Th than small (< 200-µm) sinking material (Fig. 3b,c). The geometric mean of the C:^{234}Th ratio of large sinking particles divided by that of small sinking particles was 1.6 (95% C.I. = 1.3–2.0). The C:^{234}Th ratios of swimming mesozooplankton removed from the sediment traps ranged from 25 to 855 µmol C dpm^{-1} and were, on average, 30 times greater than those of sinking material (95% C.I. = 22–41) (Fig. 3d).

We found overall satisfactory agreement between ^{234}Th flux measured by sediment trap and ^{234}Th flux estimated by a one-dimensional steady-state equation (Fig. 4). The mean ^{234}Th export flux measured by sediment traps across all cycles and depths was only 1% greater than the mean computed from ^{238}U—^{234}Th deficiency and a one-dimensional steady-state equation. The median ratio of sediment trap flux to steady-state flux was 0.89. Together, these results suggest that there was minimal bias in our sediment trap deployments. The cycle with greatest discrepancy between sediment trap and steady-state estimates was P0810 Cycle 4, during which upwelling favorable winds likely brought ^{234}Th replete waters to the surface, invalidating the assumptions of our steady-state model. The two cruises with the worst agreement between sediment trap and ^{238}U—^{234}Th deficiency-derived ^{234}Th fluxes were cruises P1106 and P1208 that sampled within and to either side of mesoscale fronts. In these dynamic regions, retention times of water within the feature (order of days) were similar to the integration temporal horizons of our sediment traps (2–4 days), but substantially shorter than the integration time of ^{238}U—^{234}Th disequilibrium (approximately one month). The mean export determined across these mesoscale features was, however, similar between the two methodologies. Because of the good agreement between sediment traps and the steady-state model, we hereafter assume that C:^{234}Th ratios determined by sediment trap accurately reflect the C:^{234}Th ratios of sinking particles. However, we cannot exclude the possibility that the sediment traps undersampled particles with low ^{234}Th.

3.3. C:^{234}Th ratio variability with depth

The C:^{234}Th ratios of sinking material typically decreased with depth. For sediment trap samples, C:^{234}Th ratios decreased with depth for 29 out of 35 samples (Fig. 5a,c). The median change with depth was −0.044 µmol C dpm^{-1} m^{-1}, with a range of −0.20 to 0.086 µmol C dpm^{-1} m^{-1}. For *in situ* pump samples, C:^{234}Th ratios decreased with depth for a similar proportion of the samples (6 out of 8, Fig. 5b,c). The median change with depth for the *in situ* pump samples was also similar (−0.056 µmol C dpm^{-1} m^{-1}, with a range of −0.12 to 0.050 µmol C dpm^{-1} m^{-1}). We tested linear, power law, and exponential functions for predicting C:^{234}Th ratios from depth. The best fit (minimum RMSE) was determined with a power law fit: C:^{234}Th = 1925 × depth$^{-1.29}$. We caution, however, that this functional form is not appropriate for extrapolating C:^{234}Th ratios to depths within the euphotic zone, because it predicts unrealistically high ratios at shallower depths than the range over which we have measurements (Fig. 5a).

To understand variability in the C:^{234}Th ratio of sinking particles, we compared the C:^{234}Th of sediment trap samples to the ratio of POC to total ^{234}Th at the trap depth and to the ratio of vertically-integrated POC to vertically-integrated total water column ^{234}Th. The latter ratio showed a very strong relationship to that of sinking particles, with Spearman's $\rho = 0.71$ ($p < 10^{-9}$). The Type II regression of the C:^{234}Th ratio of sinking particles regressed against vertically-integrated POC/vertically integrated ^{234}Th had a slope of 1.50 ± 0.10 and an intercept of 0.9 ± 0.2 µmol dpm^{-1} (Fig. 6a). The correlation of C:^{234}Th ratio of sinking particles compared to the ratio of POC to total ^{234}Th at the trap depth was weaker ($\rho = 0.53$, Fig. 6c), although still highly significant ($p = 6 \times 10^{-4}$). Furthermore, when sediment trap samples from multiple depths on the same Lagrangian cycle were compared, the variations in the ratio of vertically-integrated POC to vertically-integrated ^{234}Th were strong predictors of change in the C:^{234}Th ratios of sinking particles. This suggests that the decrease in C:^{234}Th ratios with depth may result, in part, from the facts that particles collected at deeper

Table 1
C:^{234}Th ratios (μmol dpm^{-1}) measured in sediment traps, size-fractionated sediment trap small and large fractions, swimming mesozooplankton removed from sediment trap, and > 50-μm material sampled by *in situ* pump. Mean ± standard error.

Cruise	Cycle	Depth	Sediment trap C:Th	ST ≤ 200-μm C:Th	ST ≥ 200-μm C:Th	Swimmer C:Th	*In Situ* Pump C:Th
704	1	100	5.5 ± 0.2				3.5 ± 0.2
704	2	100	3.6 ± 0.5				2.2 ± 0.1
704	4	100	7.2 ± 0.7				3.6 ± 0.7
810	1	100	10.7 ± 1				2.7 ± 0.7
810	1	50	20.5 ± 1.7				7.9 ± 4.3
810	2	100	3.3 ± 0.1				2.3 ± 0.9
810	3	100	4.2 ± 0.1				5.1 ± 3.8
810	3	60	5.6 ± 0.6				3.15
810	4	100	5.2 ± 0.5				3.97
810	4	60	7.8 ± 0.4				5.5 ± 1
810	5	100	5 ± 0.4				2.38
810	5	60	8.6 ± 0.6				4.5 ± 0.6
810	6	100	3 ± 0.2				2 ± 0.1
810	6	60	5.4 ± 1				6.61
1106	1	60	5.5 ± 0.2				2.59
1106	1	100	5.8 ± 0.4				2.65
1106	2	100	5.2 ± 0.7				1.69
1106	3	60	9.3 ± 0.5				5.27
1106	3	100	8 ± 0.1				2.92
1106	4	50	12.6 ± 0				7.63
1106	4	100	9.2 ± 1.7				3.44
1106	5	100	4.5 ± 0.3				2.75
1106	6	60	7.2 ± 0.5				
1106	6	100	6.1 ± 0.2				2.52
1208	1	60	10.9 ± 0.8	8.6 ± 0.7	26.3 ± 5.6	321	
1208	1	100	8.6 ± 0.2	6.9 ± 0.4	15.4 ± 1.1	494	
1208	2	70	6.1 ± 0.2	5.5 ± 0.2	8.94	282	
1208	2	100	8.7 ± 0.8	6.2 ± 0.6	27.2	311	
1208	3	70	10.9 ± 0.9	8.3 ± 0.7	32.01	491	
1208	3	100	7.8 ± 0.1	6.2 ± 0.1	22.32	302	
1208	4	100	3.5 ± 0.3	3.7 ± 0.1	3.3 ± 0.2		
1208	5	70	8 ± 1.2	13.8 ± 2.1	6.27		
1208	5	100	5.1 ± 0.1	7.5 ± 0.2	3.55		
1408	1	60	14.8 ± 1.4	9.6	19.62	218	
1408	1	100	8.1 ± 0.2	8.3 ± 0.3	7.8 ± 0.3	283	
1408	2	60	9.8 ± 0.7	7.1 ± 0.2	14.5 ± 1.2	120	
1408	2	100	8.7 ± 1	5.6 ± 0.4	14.3 ± 3.2	118	
1408	2	150	8 ± 1.1	5.5 ± 1.3	5.51	803	
1408	3	60	4.4 ± 0.4	3.5 ± 0.2	5.8 ± 1	74	
1408	3	100	6.7 ± 1.3	5.7 ± 1.5	4.48	161	
1408	3	150	4.1 ± 0.4	3 ± 0.5	3.98	149	
1408	4	70	4.2 ± 0.7	3.2 ± 0.8	3.88	38	
1408	4	100	2.3 ± 0.1	1.8 ± 0.1	1.81	64	
1408	4	150	2.3 ± 0.2	1.5 ± 0.3	1.9	25	
1408	5	100	4.5 ± 0.2	2.5 ± 0.2	3.72	29	
1408	5	110	2.3 ± 0.1	1.7 ± 0.1	1.3		
1408	5	150	2.6 ± 0.1	2.1 ± 0.1	1.41	46	
1604	1	100	6.1 ± 0.7	4 ± 0.8	13.87	142	
1604	1	150	2.8 ± 0.2	2.2 ± 0.2	6.88	327	
1604	2	97	6.1 ± 0.4	5.8 ± 0.6	6.82	855	
1604	2	147	4.7 ± 0.2	3.6 ± 0.2	13.57	382	
1604	3	57	10.9 ± 0.5	8.9 ± 0.7	12.8 ± 1.2	316	
1604	3	97	6.5 ± 0.5	4.9 ± 0.3	10.1 ± 1.7		
1604	3	147	4.9 ± 0.2	3.4	11.6 ± 1.7	292	
1604	4	47	8.3 ± 0.4	7.6 ± 0.1	9.1 ± 0.8		
1604	4	97	5.2 ± 0.3	4.2 ± 0.3	6.4 ± 0.4		
1604	4	147	4.3 ± 0	3.1 ± 0.3	7.5 ± 0.6		

depths integrate over a deeper water column and lower POC and higher ^{234}Th concentrations in the twilight zone than in the euphotic zone.

3.4. Relationships between C:^{234}Th ratios and biological processes

To investigate the food web and biogeochemical processes that shape the C:^{234}Th ratio of sinking particles, we first compared C:^{234}Th to the magnitude and properties of particle flux measured in the sediment traps. We found a strong correlation (Spearman's $\rho = 0.53$, $p < <10^{-3}$) between C:^{234}Th ratios of sinking particles and organic carbon flux (Fig. 7a, Table 2). C:^{234}Th increased during higher flux periods with a slope of 0.38 ± 0.015 μmol dpm^{1}/(mmol m^{-2} d^{-1}). C:^{234}Th ratio showed no statistically significant relationship to N:C ratio (Fig. 7b), but increased with increasing Si:C ratio (Spearman's $\rho = 0.42$, $p = .01$, Fig. 7c). To assess the importance of zooplankton dynamics, we compared C:^{234}Th ratios to the percentage of recognizable fecal pellet carbon in the trap. No statistically significant correlation was found with percentage fecal pellet carbon (Fig. 7d), possibly because of the relative paucity of samples (fecal pellets were only quantified on P0704, P0810, and P1604). We also compared C:^{234}Th ratios to phaeopigment flux because phaeopigments, which are chlorophyll byproducts partially produced in zooplankton guts, have previously been shown to co-vary with fecal pellets in CCE sediment traps (Morrow et al., 2018). C:^{234}Th increased with increasing

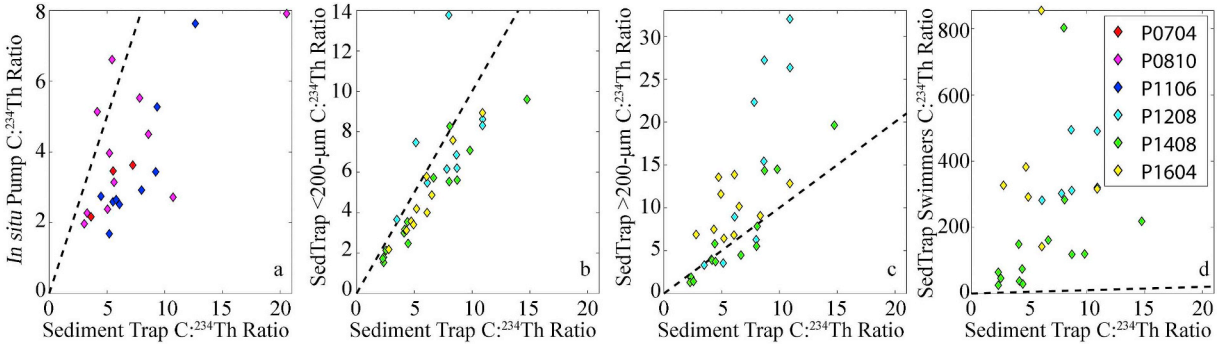

Fig. 3. Methodological variability in C:^{234}Th ratio. a) *In situ* pump C:^{234}Th ratio (typically > 50-µm), b) C:^{234}Th ratio of < 200-µm sinking material collected by sediment trap, c) C:^{234}Th ratio of > 200-µm sinking material collected by sediment trap, d) C:^{234}Th ratio of swimming mesozooplankton removed from the sediment trap. X-axis of all plots is C:^{234}Th ratio of bulk sinking material collected by sediment trap. Units are µmol C dpm^{-1}. The dashed lines indicate a 1:1 ratio.

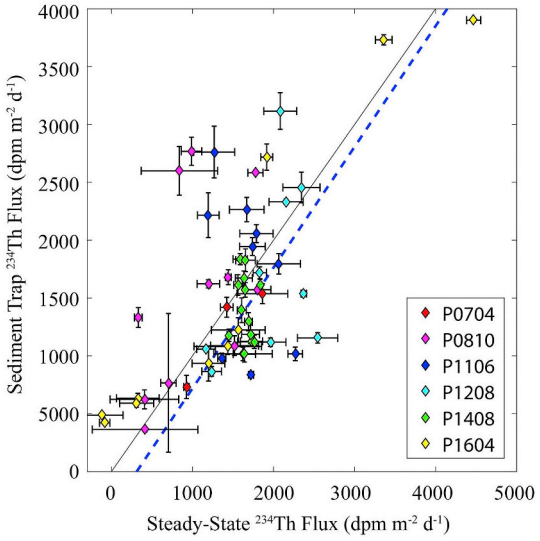

Fig. 4. Comparison of ^{234}Th flux measured by sediment trap (y-axis) to ^{234}Th estimated using ^{238}U–^{234}Th disequilibrium and a one-dimensional steady-state model. Black line is a 1:1 line. Blue dashed line is a Type II linear regression ($y = mx + b$, where $m = 1.04 \pm 0.02$ and $b = -325 \pm 41$). (For interpretation of the references to colour in this figure legend, the reader is referred to the web version of this article.)

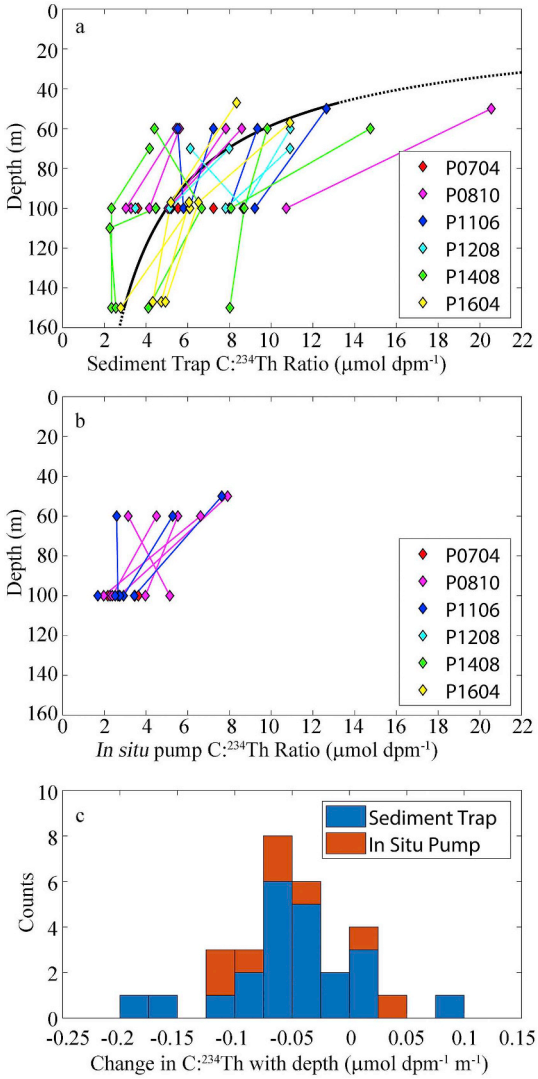

Fig. 5. C:^{234}Th ratio changes with depth. a) Sediment trap C:^{234}Th ratio plotted against depth. Lines link samples made at different depths during the same sediment trap deployment. Black line is a power law fit: C:^{234}Th = 1925 × depth$^{-1.29}$. Dotted portion of the line is outside of our data range and shows unrealistically high values within the euphotic zone. b) *In situ* pump (> 50-µm) C:^{234}Th ratio plotted against depth. c) Histogram of the change in C:^{234}Th ratio with depth.

phaeopigment:carbon ratios (Spearman's $\rho = 0.37$, $p = .007$). However, this relationship only held for low phaeopigment:carbon ratios. Above a ratio of ~100 µg Chl a equivalents/mmol C, the C:^{234}Th ratio decreased with increasing fecal pellet content (Fig. 7e). C:^{234}Th ratios increased with the percentage of the sinking particles that were retained on a 200-µm filter, although this relationship was not quite significant at the 95% C.I. (Spearman's $\rho = 0.35$, $p = .053$, Fig. 7f). This lack of statistical significance was again possibly due to a paucity of samples, because sediment trap material was only size-fractionated on three cruises.

We also compared C:^{234}Th ratios to the multiple biogeochemical and ecological measurements made in the euphotic zone (Fig. 8). For these analyses, we compared euphotic zone properties only to C:^{234}Th ratios of sinking particles at the 100-m depth horizon, because we had consistent measurements at this depth from all Lagrangian experiments. C:^{234}Th typically increased with properties that were generally indicative of higher system productivity (surface and vertically-integrated POC and Chl, percentage Chl > 20-µm, mesozooplankton biomass); however, there was no statistically significant correlation with primary production. This may be a general pattern that C:^{234}Th covaries more strongly with standing stock measurements than with rate

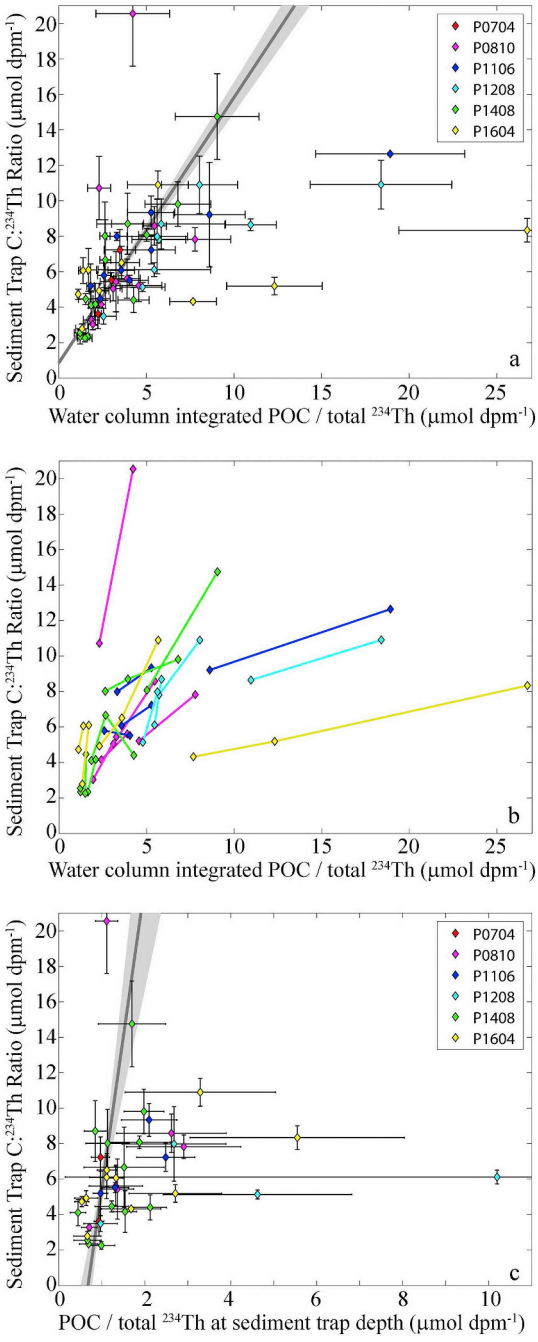

Fig. 6. C:^{234}Th ratio of sinking particles and total POC/total ^{234}Th. a) Sediment trap C:^{234}Th ratio plotted against the ratio of total vertically-integrated water column POC above the trap depth divided by total vertically-integrated ^{234}Th above the trap depth. Regression is a Type II linear regression ($y = mx + b$, where $m = 1.50 \pm 0.1$ and $b = 0.85 \pm 0.22$). b) Same as (a) but only showing samples with multiple sediment trap depths. c) Sediment trap C:^{234}Th ratio plotted against suspended POC at the trap depth divided by total ^{234}Th at the trap depth (Type II Regression: $y = mx + b$, where $m = 17.1 \pm 5.6$ and $b = -11.6 \pm 5.5$).

measurements (a statistically significant correlation was also found with mesozooplankton biomass, but not with mesozooplankton grazing rates), because standing stock measurements typically integrated over a longer period of time than plankton rate measurements. C:^{234}Th ratios decreased with the depth of the euphotic zone (1% light level) and with the depth of the nitracline, although there was no relationship between C:^{234}Th ratios and surface nitrate. Si was the only nutrient significantly correlated with the C:^{234}Th ratio, showing an inverse relationship that runs counter to the general pattern of increasing C:^{234}Th ratios in waters from recent upwelling. Silica excess (Si_{ex} = [silicic acid] – [nitrate]) was also negatively correlated with C:^{234}Th ratios. Given that regional silicic acid and nitrate in source waters are near unity, low and negative values of Si_{ex} are typically indicative of Fe-stress in the CCE (King and Barbeau, 2011). Surprisingly, despite the correlation of C:^{234}Th ratios with Si:C ratios of sinking particles and surface silicic acid, no correlation was found with percent diatom biomass, although diatom biomass was only quantified on the P0704 and P0810 cruises.

3.5. Linear models

To test the relationships between euphotic zone dynamics and the C:^{234}Th ratios of sinking particles, we used step-wise linear regression techniques. Depth, vertically-integrated POC divided by total ^{234}Th ratio (^{v}C:$^{234}Th_{tot}$), and the first three principal components of the euphotic zone properties were included as predictor variables. Step-wise linear regression was computed for each of the 1000 sets of principal component scores determined by multiple imputation. 91.5% of the linear regressions included ^{v}C:$^{234}Th_{tot}$. Each of these regressions also included PC3 (49.2%), PC2 (17.5%), or both PC2 and PC3 (24.8%). The equations for these regressions were: $\log_{10}(C{:}^{234}Th_{ST}) = 0.52 + 0.47 \times \log_{10}(^{v}C{:}^{234}Th_{tot}) + -0.032 \times PC3$; $\log_{10}(C{:}^{234}Th_{ST}) = 0.52 + 0.45 \times \log_{10}(^{v}C{:}^{234}Th_{tot}) + -0.032 \times PC2$; and $\log_{10}(C{:}^{234}Th_{ST}) = 0.52 + 0.46 \times \log_{10}(^{v}C{:}^{234}Th_{tot}) + -0.029 \times PC2 + -0.021 \times PC3$. Taken together, these results suggest that ^{v}C:$^{234}Th_{tot}$ may be the dominant driver of changing C:^{234}Th ratios of sinking material and that C:^{234}Th ratios may be higher than expected when biomass-normalized rates are low (PC2) or when the diatom community is Fe-limited (PC3). These results consistently suggest that the decline phases of blooms may have higher than typical C:^{234}Th ratios for sinking particles.

The remaining 8.5% of the regressions included depth and PC1: $\log_{10}(C{:}^{234}Th_{ST}) = 1.02 + -0.0027 \times depth + 0.037 \times PC1$. These results suggest that the C:^{234}Th ratio is positively correlated with ecosystem biomass and productivity (PC1) and decreases with depth. The absence of any models that included both ^{v}C:$^{234}Th_{tot}$ and PC1 is likely a result of strong correlation between ^{v}C:$^{234}Th_{tot}$ and PC1. The absence of models including both ^{v}C:$^{234}Th_{tot}$ and depth arises from the fact that ^{v}C:$^{234}Th_{tot}$ inherently accounts for changes in C:^{234}Th ratios with depth, because POC decreases with increasing depth below the euphotic zone, while ^{234}Th remains relatively constant.

We further investigated these relationships using bootstrapping and reduced datasets. For these reduced datasets, 50% of the data was selected at random and used to perform a multiple linear regression. The goodness of fit was assessed by predicting the C:^{234}Th ratio of the withheld data (data points not used to calculate the regression) and quantifying the model-data misfit with the RMSE. Regressions were first computed for ^{v}C:$^{234}Th_{tot}$ or depth alone to serve as baselines for determining if additional parameters added statistical power to the model. The model with ^{v}C:$^{234}Th_{tot}$ produced a lower RMSE (0.159 ± 0.020) than the model with depth (0.176 ± 0.017). The models with additional variables (PC2, PC3 or PC2 and PC3) led to slightly lower RMSE than the model with ^{v}C:$^{234}Th_{tot}$ alone (0.157 ± 0.019, 0.152 ± 0.020, and 0.150 ± 0.019, respectively), although none of these differences were significant at the 95% C.I. (*p*-values determined using non-parametric bootstrapping were 0.31, 0.18, and 0.18, respectively). The model including depth and PC1 had an RMSE of 0.147 ± 0.016 that was significantly lower than the model with depth alone ($p = .041$).

Because PC1 clearly added predictive power to the model with depth as a predictive variable, we also tested a model with $\log_{10}$(VertIntChl) as a predictive variable. Vertically-integrated Chl was chosen because it is strongly correlated with PC1, is commonly measured in field programs and had the strongest correlation with C:$^{234}Th_{ST}$ of any of the euphotic zone properties (Fig. 8, Table 3). We found that the RMSE for using vertically-integrated Chl alone (0.162 ± 0.017)

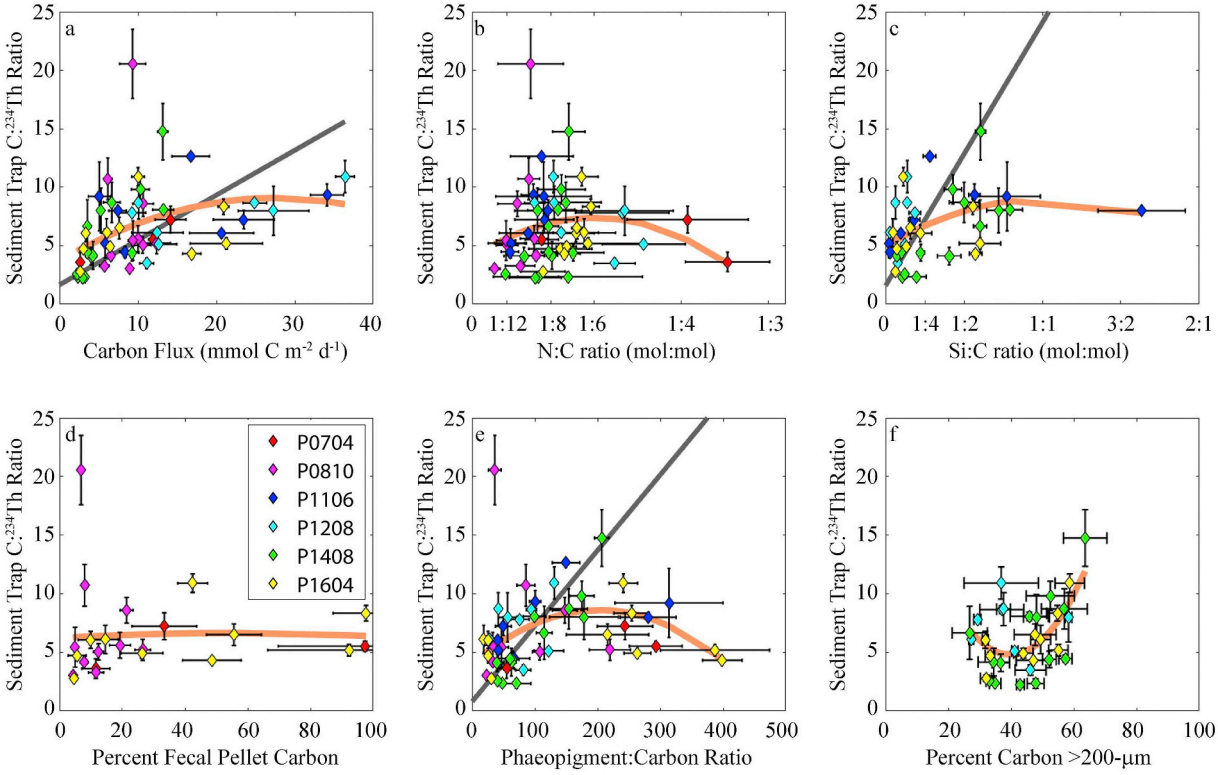

Fig. 7. C:^{234}Th ratio of sinking particles plotted against properties of sediment trap material. a) Particulate organic carbon flux. b) N:C ratio, c) Si:C ratio, d) Percentage of sinking carbon comprised of recognizable fecal pellets, e) Phaeopigment:carbon ratio (µg Chl a equivalents/mmol C). f) Percentage of sinking carbon retained on a 200-µm filter. Gray lines are Type II linear regressions (shown only for statistically significant relationships (Spearman's p-value < .05) with coefficients shown in Table 2). Light orange lines are moving polynomial regressions (LOESS smoothing).

Table 2
Relationship of C:^{234}Th ratio of sinking particles to properties of sinking flux. ρ and p-value are for Spearman's rank correlation statistics. m and b are the slope and intercept (respectively) of a Type II linear regression (see Fig. 5).

	ρ	p-value	m	b	n
C_{org} Flux	0.53	5.25E-05	0.38 ± 0.01	1.65 ± 0.1	53
N:C Ratio	0.13	0.34			53
Si:C Ratio	0.42	0.010	22.51 ± 1.18	1.57 ± 0.17	38
%Fecal Pellet Flux	0.37	0.09			23
Phaeo:C Ratio	0.37	0.007	0.06 ± 0.004	0.8 ± 0.21	51
%C > 200-µm	0.35	0.05			32

was lower than the RMSE for depth alone (0.176 ± 0.017), although the two were not statistically different. The model including depth and vertically-integrated Chl had an RMSE of 0.141 ± 0.013, which was significantly lower than that determined using depth alone (p = .016).

From these results, we concluded that the two most useful models for predicting C:^{234}Th ratios from water column properties were the model including only ^{v}C:^{234}Th$_{tot}$ and the model including both depth and vertically-integrated Chl. We used Monte Carlo uncertainty analysis to quantify uncertainty on these parameters, resulting in the equations:

$$log_{10}(C{:}\ ^{234}Th_{ST}) = a + b \times log_{10}(^{v}C{:}\ ^{234}Th_{tot}) \quad (1)$$

where a = 0.53 ± 0.02, b = 0.43 ± 0.03, and C:^{234}Th ratios are in units of µmol dpm^{-1}, and:

$$log_{10}(C{:}\ ^{234}Th_{ST}) = a + c \times depth + d \times log_{10}(VertIntChl) \quad (2)$$

where a = 0.45 ± 0.08, c = −0.0030 ± 0.0003, d = 0.37 ± 0.035, and Chl is in units of mg Chl a m^{-2}.

4. Discussion

4.1. Methodological considerations when measuring C:^{234}Th ratios

^{238}U—^{234}Th deficiency measurements of ^{234}Th export are typically converted to carbon export using C:^{234}Th ratios of sinking particles collected by sediment trap or size-fractionated particles collected by an *in situ* pump. Most frequently, the C:^{234}Th ratio of > 50-µm fraction of suspended particles is used because large particles are assumed to comprise most of the sinking flux (Buesseler et al., 2006). The disagreement between C:^{234}Th ratios of sinking particles and > 50-µm suspended particles found here (Fig. 3a) suggests that substantial uncertainty can be introduced into carbon flux measurements by the choice of particle class used for determining the C:^{234}Th ratio. C:^{234}Th ratios from sediment trap samples were typically 1.8 times greater than those of > 50-µm particles sampled by *in situ* pump. In our study region, Morrow et al. (2018) and Kelly et al. (2018) have suggested that sinking carbon flux is driven by a combination of rapidly sinking fecal pellets and slowly sinking particles that are likely heavily degraded by microbes and zooplankton as they sink. We suspect that the discrepancy between sediment trap and *in situ* pump samples is due to pump oversampling of slowly sinking particles relative to their flux contribution because these particles reside longer in the euphotic zone and shallow twilight zone than rapidly sinking material. In addition, slower sinking particles also take longer to equilibrate with the higher ^{234}Th activities beneath the euphotic zone than rapidly sinking particles, which more closely reflect the higher C:^{234}Th ratios of the euphotic zone (high POC concentrations and low ^{234}Th activities) where they are formed. We address this potential mechanism in more detail in a companion manuscript (Stukel and Kelly, this issue).

Nevertheless, there are other possible explanations for the discrepancy between > 50-µm pump and sediment trap samples. Indeed

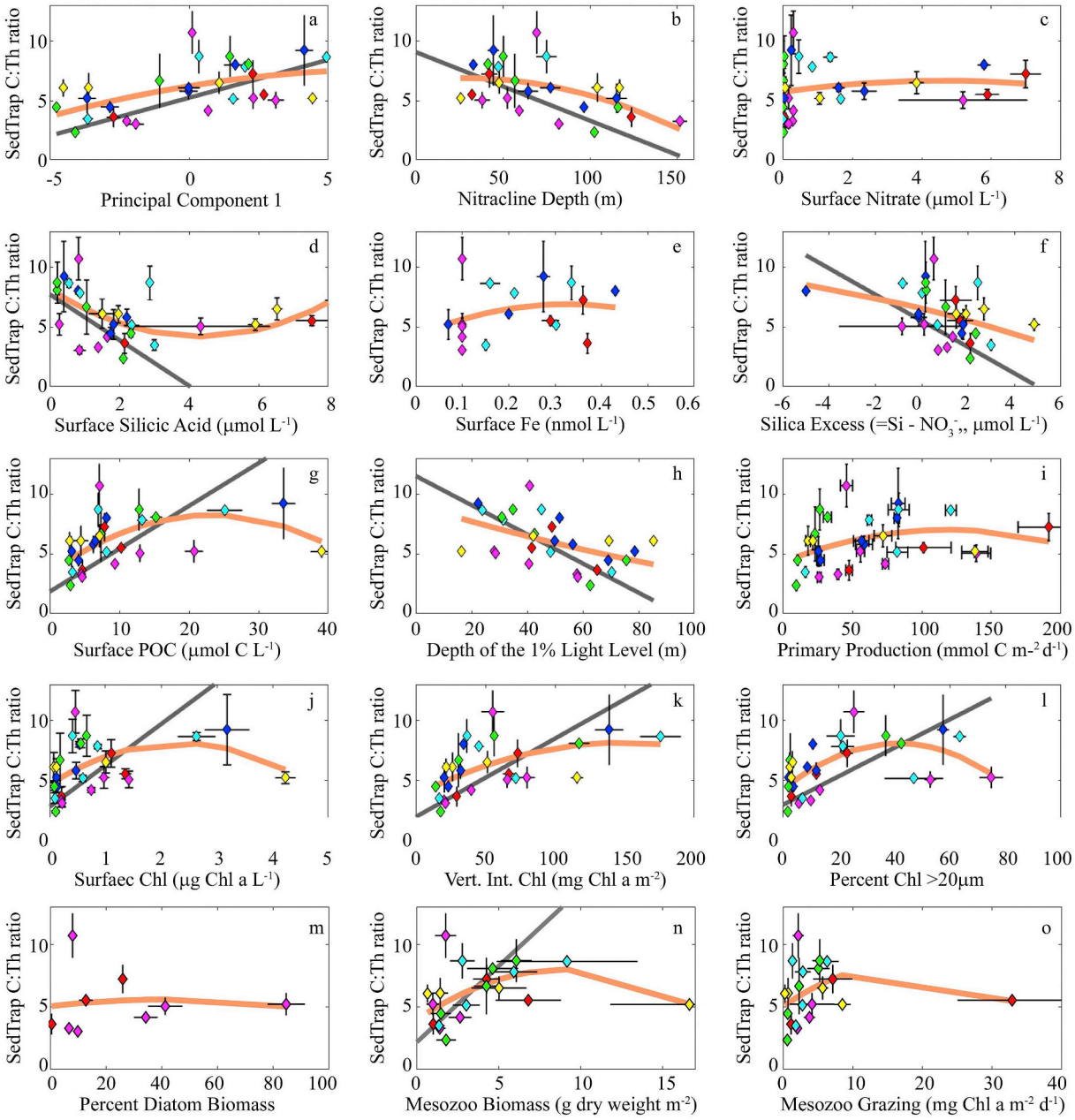

Fig. 8. C:^{234}Th ratio of sinking particles (at 100 m depth) plotted against water column measurements. a) Principal component 1. b) Nitracline depth. c) Surface NO_3^- concentration. d) Surface silicic acid concentration. e) Surface dissolved Fe. f) Surface Si_{ex} (equal to nitrate minus silicic acid). g) Surface POC. h) Depth of the euphotic zone (1% light level). i) Primary production ($^{14}HCO_3^-$ uptake). j) Surface Chl. k) Vertically-integrated Chl a. l) Percentage of total Chl a retained on a 20-μm filter. m) Diatom biomass/total phytoplankton biomass × 100. n) Mesozooplankton biomass. o) Mesozooplankton grazing (gut pigments). Gray lines are Type II linear regressions (shown only for statistically significant relationships (Spearman's p-value < .05) with coefficients shown in Table 3). Light orange lines are moving polynomial regressions (LOESS smoothing). Colors are same as Fig. 7.

the pattern that we find in the CCE is not consistent across all studies, which have shown substantial variability in the ratios of C:^{234}Th measured by sediment trap and *in situ* pump (see summaries in Buesseler et al., 2006; Hung et al., 2012). Hung et al. (2010) and Hung et al. (2012) analyzed size-fractionated sediment trap particles collected in the oligotrophic Gulf of Mexico and South China Sea and found that < 50-μm particles were responsible for most of the carbon and ^{234}Th flux. They thus concluded that a poor relationship between sediment trap C:^{234}Th ratios of sinking particles and > 50-μm *in situ* pump sampled particles occurred because the > 50-μm particles were not driving the sinking flux. However, their suggestion that the C:^{234}Th ratios of 10–50-μm particles may be more representative of sinking particles is unlikely to be the case in the CCE. Our size-fractionated sediment trap samples show that approximately half of the flux was associated with > 200-μm particles (median percentage of carbon flux attributable to > 200-μm particles was 45%, Fig. 7e). Furthermore, Stukel et al. (2018) imaged fecal pellets in CCE sediment trap samples from the P0704, P0810, and P1604 samples and found that the vast majority of the fecal pellets were > 50 μm in length.

Our belief is that the sediment trap samples accurately reflect C:^{234}Th ratios, since a comparison between sediment trap ^{234}Th flux and ^{238}U-^{234}Th-deficiency derived ^{234}Th flux suggests no substantial over- or under-collection bias. However, potential sources of sediment trap bias do exist and have been previously documented by Baker et al. (1988) and Buesseler et al. (2007). More recently, Hung et al. (2010) quantified dissolved organic carbon and dissolved ^{234}Th in unpoisoned

Table 3
Relationship of C:^{234}Th ratio of sinking particles (at 100 m depth, μmol C dpm^{-1}) to water column measurements. ρ and p-value are for Spearman's rank correlation statistics. m and b are the slope and intercept (respectively) of a Type II linear regression (see Fig. 6).

	ρ	p-value	m	b	n
Nitracline Depth (m)	−0.45	0.021	−0.06 ± 0.002	9.07 ± 0.19	29
Surface Nitrate (μmol L^{-1})	0.27	0.15			29
Surface Silicic Acid (μmol L^{-1})	−0.38	0.041	−1.91 ± 0.08	7.73 ± 0.16	29
Surface Dissolved Fe (nmol L^{-1})	0.28	0.28			26
Silica Excess (μmol L^{-1})	−0.39	0.035	−1.1 ± 0.04	5.51 ± 0.08	29
Vertically-Integrated POC (mmol m^{-2})	0.59	0.0009	0.36 ± 0.02	1.84 ± 0.11	29
Surface POC (μmol L^{-1})	0.49	0.007	−0.12 ± 0.01	11.52 ± 0.53	17
Depth of the 1% Light Level (m)	−0.48	0.009			29
Primary Production (mmol C m^{-2} d^{-1})	0.33	0.08	3.46 ± 0.17	2.78 ± 0.09	29
Surface Chl (μg L^{-1})	0.39	0.039	0.07 ± 0.003	1.92 ± 0.11	29
Vertically-Integrated Chl (mg Chl *a* m^{-2})	0.6	0.0010	0.12 ± 0.01	2.91 ± 0.08	29
% Chl > 20-μm	0.47	0.010			28
% Diatom Biomass	0.3	0.44	1.22 ± 0.2	2.17 ± 0.37	28
Mesozooplankton Biomass (g m^{-2})	0.47	0.033			29
Mesozooplankton Grazing (mg Chl *a* m^{-2} d^{-1})	0.35	0.12	−0.06 ± 0.002	9.07 ± 0.19	9

sediment traps in the Gulf of Mexico. Their results suggested that dissolution in the trap tubes may lead to the loss of half or three quarters of organic carbon or ^{234}Th (respectively) in the trap leading to a substantial under-collection bias relative to ^{238}U–^{234}Th deficiency measurements if not corrected. This is unlikely to be a serious issue for our samples, however. DNA metabarcoding analyses comparing formalin-preserved to unpreserved sediment trap samples in the CCE have shown that protistan grazers (especially dinoflagellates) grow rapidly in unpreserved sediment trap material (Gutierrez-Rodriguez et al., 2018). The activity of protists (and swimming mesozooplankton) is likely to contribute substantially to particle disaggregation and remineralization. Our sediment trap samples were deployed with a formalin brine, which should minimize such biases. The absence of a distinct under-collection bias (as determined by comparison to flux estimates from ^{238}U–^{234}Th deficiency flux estimates) suggests that any ^{234}Th loss was minor. Furthermore, on the P1408 cruise, we quantified silica dissolution in the trap tubes and found that it averaged 2.4% among all depths and cycles (median = 0.7%, range = 0.1–14.9%; Krause et al., 2015). These silica dissolution estimates likely provide an upper estimate of organic carbon dissolution in the traps, because physicochemical dissolution processes may dominate silica dissolution, while organic carbon degradation is primarily mediated by biota (inhibited by formalin) or photodegradation (insignificant at the depths of the sediment traps).

4.2. Response of C:^{234}Th ratios to plankton ecology

The nearly one order of magnitude variability in C:^{234}Th ratios of sinking particles measured in this study highlights the importance of considering variable C:^{234}Th ratios when estimating carbon flux from ^{234}Th profiles and the significant role of plankton dynamics in shaping this ratio. Two clear trends in the data were a decrease in C:^{234}Th ratio with depth and an increase in C:^{234}Th ratio with increases in total system biomass as quantified in the two equations: C:^{234}Th = 10.5 × 0.994^{depth} × PC1$^{0.037}$ and C:^{234}Th = 2.9 × 0.993^{depth} × VertIntChl$^{0.37}$. Both relationships were efficiently represented by the relationship of the C:^{234}Th ratio of sinking particles to the ratio of vertically integrated POC to vertically integrated ^{234}Th$_{tot}$ (C:^{234}Th$_{ST}$ = 3.4 × ^{v}C:^{234}Th$_{tot}^{0.44}$), because euphotic zone POC covaries strongly with ecosystem biomass, while the ratio of POC:^{234}Th$_{tot}$ decreases with depth.

Nevertheless, additional plankton ecological interactions likely influence these relationships. Step-wise linear regression consistently indicates that PC2 and/or PC3 should be included as predictor variables with ^{v}C:^{234}Th$_{tot}$. PC2 generally had near zero coefficients for plankton biomass parameters, but had positive coefficients for primary production and all surface nutrient concentrations (especially silicic acid, Fig. 2). Thus, because of the negative coefficient for PC2 in the step-wise linear regression, we surmise that actively growing blooms have lower C:^{234}Th ratios than would be expected of a mature or decaying bloom with a similar water column ^{v}C:^{234}Th$_{tot}$ ratio. Interestingly, the strongest coefficient in PC2 was for Si, while the strongest coefficient for PC3 was for Si$_{ex}$ (= [Si] – [NO_3^-]). Si$_{ex}$ is diagnostic of Fe-limitation in the CCE, which has been surmised to terminate some diatom blooms in our study region (Bruland et al., 2001; Brzezinski et al., 2015; Stukel et al., 2017). Under Fe-limitation, diatom growth, nitrogen assimilation and carbon fixation decrease, while Si uptake proceeds for a longer duration (due to reduced growth) leading to heavily silicified cells that can sink rapidly from the euphotic zone (Hutchins and Bruland, 1998; Takeda, 1998). The negative coefficients in the step-wise regressions for PC2 (most strongly driven by silicic acid concentrations) and PC3 (most strongly driven by Si$_{ex}$), suggest that diatom Fe-limitation (and subsequent sinking) may lead to increased C:^{234}Th ratios. This supposition is consistent with our finding that C:^{234}Th ratios were positively correlated with sediment trap Si:C ratios (Fig. 7c). The mechanistic link between Fe-limitation and increased C:^{234}Th ratios may be increased sinking speeds of heavily ballasted aggregates and/or fecal pellets that lead to a greater contribution of fresh, mixed-layer organic matter to carbon flux at deeper depth.

Mesozooplankton fecal pellets are one of the dominant forms of sinking particles in the CCE (Morrow et al., 2018; Stukel et al., 2013). Notably, while C:^{234}Th ratios are positively correlated with percent fecal pellet carbon and phaeopigment:carbon ratios in the sediment trap and with mesozooplankton biomass (Figs. 7d,e and 8n), at higher concentrations of fecal pellets, phaeopigments, or biomass, the relationship plateaus or reverses. To disentangle the direct effect of packaging particles into fecal pellets from the indirect effect of the covariance of zooplankton biomass and grazing with ecosystem productivity, we computed predicted sinking particle C:^{234}Th ratios from the relationships in Eqs. (1) and (2). We then compared the residuals of these predictions (relative to measured C:^{234}Th) against the percentage of fecal pellet carbon in the sediment trap (Supp. Fig. 1c,d). While the correlation between the residual and % fecal pellet carbon was not significant, it was negative for both C:^{234}Th relationships. By computing the Type II slope of the normalized residual plotted against % fecal pellet carbon, we can assess the percentage change in C:^{234}Th ratio with increasing fecal pellet composition in the sediment traps (Supp. Fig. 1e,f). The slope of this regression was −0.36 ± 0.01 with ^{v}C:^{234}Th$_{tot}$ used as the predictor variable or − 0.26 ± 0.19 with depth and vertically-integrated Chl. These values suggest that when the proportion of fecal pellets in the sample increases from 0% to 100%, the C:^{234}Th ratios decrease by 36% or 26%. This is consistent with a situation in which zooplankton consume particles and preferentially

digest the carbon within them, while most or all of the ^{234}Th passes through their guts into fecal pellets as has been observed for other actinide elements (Reinfelder and Fisher, 1991). This possibility is further supported by the high C:^{234}Th of zooplankton measured in this study (Fig. 3d) and others (Coale, 1990; Dunne et al., 2000; Passow et al., 2006; Stukel et al., 2016). Experimental studies showing that the ^{234}Th found in crustaceans can bioaccumulate directly from dissolved ^{234}Th further supports this supposition (Rodriguez y Baena et al., 2008; Rodriguez y Baena et al., 2006).

Although not specifically addressed in our study, microbial degradation of sinking particles also likely plays a substantial role in modifying the C:^{234}Th ratios of bulk sinking material. Respiration of particle-attached bacteria is a substantial source of flux attenuation in the twilight zone and likely leads to preferential degradation of carbon (relative to thorium) and hence a decrease in C:^{234}Th ratios with depth (Buesseler et al., 2006; Simon et al., 2002). This simple conceptual view may be complicated, however, by microbial interactions including quorum sensing (Hmelo, 2017; Mislan et al., 2014) and production or breakdown of thorium binding ligands by bacteria (Hirose and Tanoue, 2001; Quiroz et al., 2006; Santschi et al., 2003). Furthermore, the presence of flux feeders, including Rhizaria that are abundant in the CCE (Biard et al., 2018; Stukel et al., 2018), may lead to flux attenuation without a substantial change in C:^{234}Th ratios. The relative importance of particle-attached microbes and flux feeding zooplankton in modifying C:^{234}Th ratios in the mesopelagic zone thus deserves further study.

Similarly, aggregation may play an important role in C:^{234}Th ratios that could not be determined from this study. A null hypothesis might be that aggregation should not change the relationship between C:^{234}Th and particle size (Buesseler et al., 2006). However, acidic polysaccharides have a high affinity for Th, leading to a strong correlation between C:^{234}Th ratios and transparent exopolymers that are believed to play an important role in aggregation (Passow et al., 2006; Quigley et al., 2002; Santschi et al., 2003). Furthermore, colloidal pre-cursors of aggregates can be substantially enriched in ^{234}Th (Guo and Santschi, 1997). Conflicting results relating particle size to C:^{234}Th ratios and the multiplicity of processes that can influence aggregation and the particle size spectrum thus suggest that additional investigation of aggregation-C:^{234}Th relationships is needed (Buesseler et al., 2006; Burd et al., 2007; Santschi et al., 2006).

4.3. Comparison of CCE C:^{234}Th ratios to other regions

The range of variation in productivity encountered in the CCE during our study is nearly as great as that typically found globally (*e.g.*, globally, sea surface Chl derived from a SeaWIFS annual climatology ranges from ~0.02 to ~10 μg Chl *a* L^{-1}; average sea surface Chl *a* measured on cycles in this study ranged from 0.07 to 4.2 μg Chl *a* L^{-1}). Given this large range in ecosystem productivity, it is worth considering how C:^{234}Th ratios measured in this study compare to ranges of C:^{234}Th variability encountered in other studies. Our goal in this section is not to exhaustively review C:^{234}Th ratios (for more thorough discussions, we refer readers to Buesseler et al., 2006; Burd et al., 2007; Hung et al., 2012). Rather, we ask whether the patterns that we have found for the CCE are consistent with those found in other regions.

In a comprehensive review of C:^{234}Th ratios, Buesseler et al. (2006) noted that C:^{234}Th ratios were typically < 5 in oligotrophic regions and > 10 in productive coastal areas. More recently, Hung et al. (2012) tabulated results from studies around the globe and found estimates of sediment trap-derived C:^{234}Th ratios in the twilight zone ranging from ~1 to 25 μmol dpm^{-1}, with the exception of the Baltic Sea, which had higher C:^{234}Th ratios as a result of low ^{238}U activity. Hung et al. (2010) used sediment traps and *in situ* pumps to collect particles from the Gulf of Mexico, East China Sea, and Northwest Pacific. At depths ranging from 65 to 140 m, they found sediment trap-derived C:^{234}Th ratios that ranged from 0.8 to 20 μmol dpm^{-1}. They also found that the C:^{234}Th ratios of suspended particles were very different for different size classes, with small (1–10 μm) and large (> 150 μm) particles having highly variable C:^{234}Th ratios that could be nearly two orders of magnitude higher than the C:^{234}Th ratios of intermediately sized particles (10–50 μm and 50–150 μm).

Owens et al. (2015) used *in situ* pumps to sample > 51-μm particles on GEOTRACES cruises in the North and South Atlantic. They measured C:^{234}Th at up to 16 depths per station and fit a power law relationship to data from ~75 to 250 m depth and found that on average C:^{234}Th = 135.3 × depth$^{-0.795}$. Although the exponent computed for the Atlantic differs from the exponent that we quantified for a power law fit (−1.29) this difference is caused more by a different depth range used for the regression (40–150 m for our samples). Indeed at similar depth ranges, C:^{234}Th ratios in the North Atlantic were comparable to those in the CCE. At depths of 50 m or shallower, Owens et al. (2015) measured C:^{234}Th ratios ranging from ~3 to 21 μmol dpm^{-1}, compared to our sediment trap measurements of ~4–21 μmol dpm^{-1}for depths of 40–60 m. At ~100 m, Atlantic C:^{234}Th ratios varied from ~2–6 μmol dpm^{-1}, compared to our measurements of 2.3–10.7 μmol dpm^{-1} using sediment traps and 1.7–5.8 μmol dpm^{-1} using *in situ* pumps.

Maiti et al. (2016) used sediment traps and *in situ* pumps to measure C:^{234}Th ratios in the Gulf of Mexico after the Deepwater Horizon oil spill. They found good agreement between sediment traps and > 51-μm suspended material with C:^{234}Th ratios ranging from 7 to 10 μmol dpm^{-1} at 100-m depth and decreasing to < 1 to 3 μmol dpm^{-1} at 350 m. Over these depth ranges, they fit power law relationships to the *in situ* pump data with exponents of −1.36 in 2012 and − 0.84 in 2013.

In areas closer to our study region, Benitez-Nelson et al. (2001) measured C:^{234}Th monthly in sediment traps at a depth of 150 m at Station ALOHA (North Pacific Subtropical Gyre) and found a range of 3.5–15 μmol dpm^{-1} (although only a single sample exceeded 6 μmol dpm^{-1}). Maiti et al. (2008) measured C:^{234}Th ratios in sediment traps (also at 150 m) within (1.5 μmol dpm^{-1}) and outside of (2.7 μmol dpm^{-1}) a cyclonic eddy near Station ALOHA. Buesseler et al. (2009) used neutrally-buoyant and surface-tethered sediment traps to measure C:^{234}Th ratios at 150, 300, and 500 m at Stations ALOHA and K2 (high-nutrient, low-chlorophyll site in the North Pacific Subarctic Gyre). They found good agreement between the two methods and a consistent decrease in C:^{234}Th with depth at both sites. At Station ALOHA, C:^{234}Th declined from 3 to 7 μmol dpm^{-1} at 150 m to 1–2 μmol dpm^{-1} at 500 m. At K2 the 150 m values were slightly lower (3–5 μmol dpm^{-1}) while the deeper values were also ~1–2 μmol dpm^{-1}. In the Costa Rica Upwelling Dome (Eastern Tropical North Pacific), Stukel et al. (2016) measured C:^{234}Th ratios of 3.7 to 11.6 μmol dpm^{-1} at 90–100 m depth and 3.1–10.2 μmol dpm^{-1} at 150 m depth.

To assess whether Eq. (1) was a reasonable predictor of C:^{234}Th, we found publicly available datasets for which drifting sediment trap C:^{234}Th values, POC profiles, and ^{234}Th profiles were all available. Four such datasets were found from the Sargasso Sea EDDIES program (Buesseler et al., 2008), the VERTIGO program study site at K2 in the North Pacific Subarctic Gyre (Buesseler et al., 2009), the Costa Rica Dome (Stukel et al., 2016), and the Western Antarctic Peninsula (Buesseler et al., 2010; Owens, 2013). Results showed strong agreement between these globally-dispersed datasets and Eq. (1) (Fig. 9). This gives us some confidence that ^{v}C:^{234}Th$_{tot}$ may be a valuable predictor of C:^{234}Th ratios of particles globally, although we caution that, whenever possible, C:^{234}Th ratios should still be determined empirically.

4.4. Thorium sorption models

The goal of predicting variability in C:^{234}Th ratios, and their impact on carbon flux calculations determined from ^{238}U—^{234}Th disequilibrium, depends on development of mechanistic ^{234}Th sorption models that are simple enough to be applied to (and validated against)

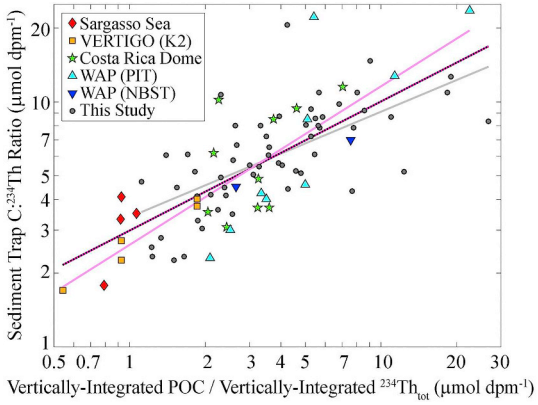

Fig. 9. Comparison of the relationship of $^{v}C{:}^{234}Th_{tot}$ (x-axis) with $C{:}^{234}Th$ ratios of sinking particles for additional regions around the globe including the Sargasso Sea (Buesseler et al., 2008), the Subarctic Pacific (K2, Buesseler et al., 2009), the Costa Rica Dome (Stukel et al., 2016), and the Western Antarctic Peninsula (WAP, Owens, 2013). The light gray line is the regression for data from this study only (see Eq. (1)). The light magenta line is the regression line from all other data sets combined: $\log_{10}(C{:}^{234}Th_{ST}) = m \times \log_{10}(^{v}C{:}^{234}Th_{tot}) + b$, where $m = 0.65 \pm 0.18$ and $b = 0.42 \pm 0.01$ ($R^2 = 0.65$, $p < < 10^{-6}$). The dashed magenta-black line is a regression combining our data with these additional datasets:$\log_{10}(C{:}^{234}Th_{ST}) = m \times \log_{10}(^{v}C{:}^{234}Th_{tot}) + b$, where $m = 0.53 \pm 0.10$ and $b = 0.48 \pm 0.06$ ($R^2 = 0.55$, $p < < 10^{-6}$). (For interpretation of the references to colour in this figure legend, the reader is referred to the web version of this article.)

typical *in situ* measurements. Models of varying complexity have been applied, including those with and without explicit desorption, aggregation through a colloidal pre-cursor, multiple size classes of particles, different chemical constituents within particles, and coupling to phytoplankton dynamics (Burd et al., 2007; Dunne et al., 1997; Honeyman et al., 1988; Savoye et al., 2006). At a basic level, particulate ^{234}Th (Th_{par}) activity (units of dpm m^{-3}) can be modeled as a balance between scavenging of dissolved ^{234}Th (Th_{dis}) and losses to desorption, decay, and sinking:

$$\frac{\partial Th_{par}}{\partial t} = k_1 Th_{dis} POC - \lambda_{234} Th_{par} - k_{-1} Th_{par} - \frac{\partial E_{Th}}{\partial z} \quad (3)$$

where, k_1 and k_{-1} are the thorium sorption and desorption constants, respectively, λ_{234} is the decay constant for ^{234}Th, and E_{Th} is vertical export of sinking Th_{par} (see, *e.g.*, Eq. (8) of Dunne et al., 1997). While this model oversimplifies the complex interactions between ^{234}Th and binding sites on different organic molecules and particulate size fractions, it provides a useful starting point for examining sorption dynamics. If we assume that the surface ocean is a well-mixed layer, $\partial E_{Th}/\partial z$ can be rewritten as the export of Th out of the bottom of the layer divided by the thickness of the layer ($E_{Th}/\Delta z$). We will define φ as the inverse of the turnover time of POC (or Th_{par}) with respect to sinking, thus: $\varphi = E_{POC}/\Delta z/POC = E_{Th}/\Delta z/Th_{par}$). If we assume steady state, we can re-write Eq. (3) as:

$$k_1 Th_{dis} POC = (\lambda_{234} + k_{-1} + \varphi) Th_{par} \quad (4)$$

and rearrange to calculate the $C{:}^{234}Th$ ratio of particles in the layer (which must be equal to the $C{:}^{234}Th$ ratio of particles sinking out of the layer):

$$C{:}\,^{234}Th_{sink} = \frac{POC}{Th_{par}} = \frac{\lambda_{234} + k_{-1} + \varphi}{k_1 Th_{dis}} \quad (5)$$

Since $Th_{par} + Th_{dis}$ is equal to the total ^{234}Th in the water column (Th_{tot}), we can show:

$$C{:}\,^{234}Th_{sink} = \frac{POC}{Th_{tot}} + \frac{\lambda_{234} + k_{-1} + \varphi}{k_1 Th_{tot}} \quad (6)$$

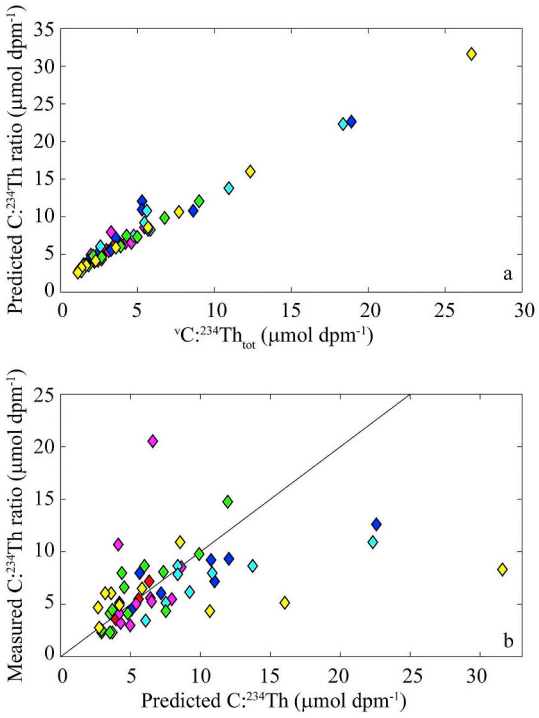

Fig. 10. – One-layer, two-box thorium sorption, desorption, and sinking model (see Eqs. (3)–(6). a) Relationship between vertically-integrated POC to vertically-integrated total water column ^{234}Th (x-axis) and model predictions (y-axis). b) Measured $C{:}^{234}Th$ of sinking particles plotted against model predictions (using $k_1 = 0.013$). Black line is 1:1 line.

Eq. (6) explains the strong correlation between $C{:}^{234}Th$ ratios of sinking particles (equal to $C{:}^{234}Th_{sink}$ in Eq. (6)) and $^{v}POC{:}^{234}Th_{tot}$ (equal to POC/Th_{tot} in Eq. (6)). Typical values for the constants in these equations are: $\lambda = 0.029$ d^{-1}, $k_1 = 0.006\ m^3\ mmol\ C^{-1}\ d^{-1}$, and $k_{-1} = 0.01\ d^{-1}$ (Murnane et al., 1994; Resplandy et al., 2012), while our field data suggests that φ is generally in the range of 0.01 to 0.02 d^{-1}. Based on these values, $(\lambda + k_{-1} + \varphi)/k_1$ should range from ~4 to 8 mmol C m^{-3}, which is of the same order of magnitude of measured vertically-averaged POC on our cycles (2.4 to 24 mmol C m^{-3}). This suggests that the $C{:}^{234}Th$ ratio of sinking particles should vary approximately linearly with the ratio of vertically-integrated POC to vertically-integrated $^{234}Th_{tot}$ (in agreement with our results in Fig. 6a). The relationship between $^{v}C{:}^{234}Th_{tot}$ and predicted $C{:}^{234}Th$ ratios is shown in Fig. 10a.

Eq. 6 gives a mechanistic explanation for the empirical relationships underlying Fig. 6a and Eq. (2), but it can also be inverted to estimate the thorium adsorption coefficient (k_1). Using the data from each Lagrangian experiment to calculate the adsorption coefficient, we found a median k_1 of 0.013 m^3 mmol C^{-1} d^{-1}, with an interquartile range of 0.0057 to 0.0216. This wide range likely reflects true variability in the adsorption coefficient in a dynamic upwelling biome. Adsorption coefficients can vary with the concentration of acidic polysaccharides and other organic ligands, pH, temperature, and the presence of inorganic particles (Passow et al., 2006; Quigley et al., 2002; Santschi et al., 2006). However, there is also substantial uncertainty associated with our use of a simple steady-state, one-layer, two-box model, without aggregation processes mediated by colloidal particles. More complex models (*e.g.*Burd et al., 2007; Dunne et al., 1997) may more accurately explain ^{234}Th-particle dynamics, but could not be constrained with our *in situ* data.

Despite the simplicity of the model used in Eq. (3), the results (when computed using the median adsorption coefficient of k_1, 0.013), showed good agreement to the measured data for predicted values of $C{:}^{234}Th < 15$ μmol dpm $^{-1}$ (Fig. 10b). The RMSE for the model (after

$\log_{10}$ transformation to be consistent with linear models in section 3.5) was 0.20. Although this was higher than the RMSE of the best-fit empirical models (RMSE = 0.14 for depth and vertically-integrated Chl and RMSE = 0.16 for ^{v}C:$^{234}Th_{tot}$), it is encouraging that this un-tuned, mechanistic model delivers realistic estimates of the C:^{234}Th ratios of sinking particles. This gives hope that mechanistic and/or empirical relationships from future studies will provide better results than simple averaging or linear extrapolation between sparse *in situ* measurements of C:^{234}Th. Such results could substantially improve understanding of spatial and temporal variability in the biological pump. Nevertheless, it is clear that significant unexplained variance in the data remains. Future experiments that explicitly link thorium adsorption kinetics to *in situ* chemistry and plankton ecology are clearly needed.

Acknowledgments

We thank the captains and crew of the R/*Vs Melville*, *T.G. Thompson*, and *Sikuliaq* for making this work possible. We also thank Drs. Peter Morton and Vincent Salters for assistance with ICP-MS measurements and Dr. Claudia Benitez-Nelson for extensive assistance with ^{234}Th analyses on the P0704, P0810, and P1106 Cruises. We are deeply indebted to our many colleagues within the CCE LTER who contributed to sample collection and analysis. Data used in this manuscript are freely available on the CCE LTER Datazoo website: https://oceaninformatics.ucsd.edu/datazoo/catalogs/ccelter/datasets. This work was supported by NSF Biological Oceanography grants to the CCE LTER Program: OCE-0417616, OCE-1026607, OCE-1637632, and OCE-1614359. A portion of this work was performed at the National High Magnetic Field Laboratory, which is supported by National Science Foundation Cooperative Agreement No. DMR-1644779 and the State of Florida.

Appendix A. Supplementary data

Supplementary data to this article can be found online at https://doi.org/10.1016/j.marchem.2019.01.003.

References

Baker, E.T., Milburn, H.B., Tennant, D.A., 1988. Field assessment of sediment trap efficiency under varying flow conditions. J. Mar. Res. 46 (3), 573–592.
Benitez-Nelson, C., Buesseler, K.O., Karl, D.M., Andrews, J., 2001. A time-series study of particulate matter export in the North Pacific Subtropical Gyre based on Th-234 : U-238 disequilibrium. Deep-Sea Res I 48 (12), 2595–2611.
Benitez-Nelson, C.R., et al., 2001. Testing a new small-volume technique for determining Th-234 in seawater. J. Radioanal. Nucl. Chem. 248 (3), 795–799.
Biard, T., Krause, J.W., Stukel, M.R., Ohman, M.D., 2018. The significance of giant Phaeodarians (Rhizaria) to biogenic silica export in the California current ecosystem. Glob. Biogeochem. Cycles 32 (6), 987–1004.
Black, E.E., Buesseler, K.O., Pike, S.M., Lam, P.J., 2017. ^{234}Th as a tracer of particulate export and remineralization in the southeastern tropical Pacific. Mar. Chem. 201, 35–50.
Bruland, K.W., Rue, E.L., Smith, G.J., 2001. Iron and macronutrients in California coastal upwelling regimes: Implications for diatom blooms. Limnol. Oceanogr. 46 (7), 1661–1674.
Brzezinski, M.A., et al., 2015. Enhanced silica ballasting from iron stress sustains carbon export in a frontal zone within the California current. J Geophys Res Oceans 120 (7), 4654–4669.
Buesseler, K.O., Bacon, M.P., Cochran, J.K., Livingston, H.D., 1992. Carbon and nitrogen export during the JGOFS North Atlantic bloom experiment estimated from ^{234}Th:^{238}U disequilibria. Deep-Sea Res. 39 (7-8A), 1115–1137.
Buesseler, K.O., Boyd, P.W., 2009. Shedding light on processes that control particle export and flux attenuation in the twilight zone of the open ocean. Limnol. Oceanogr. 54 (4), 1210–1232.
Buesseler, K.O., McDonnell, A.M.P., Schofield, O.M.E., Steinberg, D.K., Ducklow, H.W., 2010. High particle export over the continental shelf of the West Antarctic Peninsula. Geophys. Res. Lett. 37.
Buesseler, K.O., et al., 2006. An assessment of particulate organic carbon to thorium-234 ratios in the ocean and their impact on the application of ^{234}Th as a POC flux proxy. Mar. Chem. 100 (3–4), 213–233.
Buesseler, K.O., et al., 2007. An assessment of the use of sediment traps for estimating upper ocean particle fluxes. J. Mar. Res. 65 (3), 345–416.
Buesseler, K.O., et al., 2008. Particle fluxes associated with mesoscale eddies in the Sargasso Sea. Deep-Sea Res Part Ii-Topical Studies Oceanograph 55 (10 − 13), 1426–1444.
Buesseler, K.O., et al., 2009. Thorium-234 as a tracer of spatial, temporal and vertical variability in particle flux in the North Pacific. Deep-Sea Res. I Oceanogr. Res. Pap. 56 (7), 1143–1167.
Burd, A.B., Jackson, G.A., Moran, S.B., 2007. The role of the particle size spectrum in estimating POC fluxes from Th-234/U-238 disequilibrium. Deep-Sea Res I 54 (6), 897–918.
Buuren, S.v., Groothuis-Oudshoorn, K., 2010. Mice: multivariate imputation by chained equations in R. J. Stat. Softw. 1–68.
Chen, J.H., Edwards, R.L., Wasserburg, G.J., 1986. ^{238}U, ^{234}U and ^{232}Th in seawater. Earth Planet. Sci. Lett. 80 (3–4), 241–251.
Coale, K.H., 1990. Labyrinth of doom: a device to minimize the swimmer component in sediment trap collections. Limnol. Oceanogr. 35 (6), 1376–1381.
Coale, K.H., Bruland, K.W., 1985. Th-234 - U-238 Disequilibria within the California Current. Limnol. Oceanogr. 30 (1), 22–33.
van der Loeff, M.R., et al., 2011. Th-234 in surface waters: distribution of particle export flux across the Antarctic Circumpolar current and in the Weddell Sea during the GEOTRACES expedition ZERO and DRAKE. Deep-Sea Res Part Ii-Topical Studies Oceanograph 58 (25–26), 2749–2766.
Ducklow, H.W., Steinberg, D.K., Buesseler, K.O., 2001. Upper Ocean carbon export and the biological pump. Oceanography 14 (4), 50–58.
Ducklow, H.W., et al., 2018. Spring-summer net community production, new production, particle export and related water column biogeochemical processes in the marginal sea ice zone of the Western Antarctic Peninsula 2012–2014. Philos. Trans. R. Soc. Lond. A 376.
Dunne, J.P., Armstrong, R.A., Gnanadesikan, A., Sarmiento, J.L., 2005. Empirical and mechanistic models for the particle export ratio. Glob. Biogeochem. Cycles 19 (4), GB4026.
Dunne, J.P., Murray, J.W., Rodier, M., Hansell, D.A., 2000. Export flux in the western and central equatorial Pacific: zonal and temporal variability. Deep-Sea Res I 47 (5), 901–936.
Dunne, J.P., Murray, J.W., Young, J., Balistrieri, L.S., Bishop, J., 1997. Th-234 and particle cycling in the central equatorial Pacific. Deep-Sea Res Part Ii-Topical Studies Oceanograph 44 (9–10), 2049–2083.
Durkin, C.A., Estapa, M.L., Buesseler, K.O., 2015. Observations of carbon export by small sinking particles in the upper mesopelagic. Mar. Chem. 175, 72–81.
Estapa, M.L., et al., 2015. Decoupling of net community and export production on submesoscales. Glob. Biogeochem. Cycles 29 (8), 1266–1282.
Goericke, R., 2011. The size structure of marine phytoplankton - What are the rules? In: California Cooperative Oceanic Fisheries Investigations Reports. Vol. 52. pp. 198–204.
Goericke, R., Ohman, M.D., 2015. Introduction to CCE-LTER: responses of the California Current Ecosystem to climate forcing. Deep-Sea Res. II Top. Stud. Oceanogr. 112, 1–5.
Guo, L., Hung, C.-C., Santschi, P.H., Walsh, I.D., 2002. 234Th scavenging and its relationship to acid polysaccharide abundance in the Gulf of Mexico. Mar. Chem. 78 (2–3), 103–119.
Guo, L., Santschi, P.H., 1997. Composition and cycling of colloids in marine environments. Rev. Geophys. 35 (1), 17–40.
Gutierrez-Rodriguez, A., et al., 2018. High contribution of Rhizaria (Radiolaria) to vertical export in the California Current Ecosystem revealed by DNA metabarcoding. ISME J. https://doi.org/10.1038/s41396-018-0322-7. (in press).
Henson, S.A., et al., 2011. A reduced estimate of the strength of the ocean's biological carbon pump. Geophys. Res. Lett. 38.
Hirose, K., Tanoue, E., 2001. Strong ligands for thorium complexation in marine bacteria. Mar. Environ. Res. 51 (2), 95–112.
Hmelo, L.R., 2017. Quorum sensing in marine microbial environments. Annu. Rev. Mar. Sci. 9, 257–281.
Honeyman, B.D., Balistrieri, L.S., Murray, J.W., 1988. Oceanic trace metal scavenging: the importance of particle concentration. Deep Sea Res Part A. Oceanograph Res Papers 35 (2), 227–246.
Hung, C.C., Gong, G.C., Santschi, P.H., 2012. Th-234 in different size classes of sediment trap collected particles from the Northwestern Pacific Ocean. Geochim. Cosmochim. Acta 91, 60–74.
Hung, C.C., et al., 2010. Comparative evaluation of sediment trap and Th-234-derived POC fluxes from the upper oligotrophic waters of the Gulf of Mexico and the subtropical northwestern Pacific Ocean. Mar. Chem. 121 (1–4), 132–144.
Hutchins, D.A., Bruland, K.W., 1998. Iron-limited diatom growth and Si: N uptake ratios in a coastal upwelling regime. Nature 393 (6685), 561–564.
Kahru, M., Jacox, M.G., Ohman, M.D., 2018. CCE1: Decrease in the frequency of oceanic fronts and surface chlorophyll concentration in the California Current System during the 2014–2016 Northeast Pacific warm anomalies. Deep-Sea Res. I Oceanogr. Res. Pap. 140, 4–13.
Kelly, T.B., Goericke, R., Kahru, M., Song, H., Stukel, M.R., 2018. CCE II: spatial and interannual variability in export efficiency and the biological pump in an eastern boundary current upwelling system with substantial lateral advection. Deep Sea Res I 140, 14–25.
King, A.L., Barbeau, K.A., 2011. Dissolved iron and macronutrient distributions in the southern California Current System. J. Geophys. Res. Oceans 116.
Knauer, G.A., Martin, J.H., Bruland, K.W., 1979. Fluxes of particulate carbon, nitrogen, and phosphorus in the upper water column of the Northeast Pacific. Deep-Sea Res. 26 (1), 97–108.
Krause, J.W., et al., 2015. Variability in diatom contributions to biomass, organic matter production and export across a frontal gradient in the California Current Ecosystem. J. Geophys. Res. Oceans 120 (2), 1032–1047.
Landry, M.R., Ohman, M.D., Goericke, R., Stukel, M.R., Tsyrklevich, K., 2009. Lagrangian studies of phytoplankton growth and grazing relationships in a coastal upwelling ecosystem off Southern California. Prog. Oceanogr. 83, 208–216.

Landry, M.R., et al., 2012. Pelagic community responses to a deep-water front in the California Current Ecosystem: overview of the A-Front Study. J. Plankton Res. 34 (9), 739–748.
Laws, E.A., D'Sa, E., Naik, P., 2011. Simple equations to estimate ratios of new or export production to total production from satellite-derived estimates of sea surface temperature and primary production. Limnology Oceanograph-Methods 9, 593–601.
Le Moigne, F.A.C., Henson, S.A., Madsen, E., 2013. Global database of surface ocean particulate organic carbon export fluxes diagnosed from the 234Th technique. Earth Syst Sci Data 5, 295–304.
Lepore, K., et al., 2009. Sediment trap and in-situ pump size-fractionated POC/234Th ratios in the Mediterranean Sea and Northwest Atlantic: implications for POC export. Deep-Sea Res. I Oceanogr. Res. Pap. 56 (4), 599–613.
Maiti, K., Benitez-Nelson, C.R., Rii, Y., Bidigare, R., 2008. The influence of a mature cyclonic eddy on particle export in the lee of Hawaii. Deep-Sea Res Part Ii-Topical Studies Oceanograph 55 (10–13), 1445–1460.
Maiti, K., et al., 2016. Export fluxes in northern Gulf of Mexico – comparative evaluation of direct, indirect and satellite-based estimates. Mar. Chem. 184, 60–77.
McDonnell, A.M.P., Buesseler, K.O., 2010. Variability in the average sinking velocity of marine particles. Limnol. Oceanogr. 55 (5), 2085–2096.
McDonnell, A.M.P., et al., 2015. The oceanographic toolbox for the collection of sinking and suspended marine particles. Prog. Oceanogr. 133, 17–31.
Mislan, K.A.S., Stock, C.A., Dunne, J.P., Sarmiento, J.L., 2014. Group behavior among model bacteria influences particulate carbon remineralization depths. J. Mar. Res. 72 (3), 183–218.
Morrow, R.M., et al., 2018. Primary productivity, Mesozooplankton grazing, and the biological pump in the California Current Ecosystem: variability and response to El Niño. Deep-Sea Res. I (140), 52–62.
Murnane, R., Cochran, J., Sarmiento, J., 1994. Estimates of particle-and thorium-cycling rates in the Northwest Atlantic Ocean. J. Geophys. Res. 99 (C2), 3373–3392.
Murphy, R.J., Lenhart, J.J., Honeyman, B.D., 1999. The sorption of thorium (IV) and uranium (VI) to hematite in the presence of natural organic matter. Colloids Surf. A Physicochem. Eng. Asp. 157 (1–3), 47–62.
Murray, J.W., et al., 1996. Export flux of particulate organic carbon from the central equatorial Pacific determined using a combined drifting trap Th-234 approach. Deep-Sea Res Part Ii-Topical Studies Oceanograph 43 (4–6), 1095–1132.
Nickels, C.F., Ohman, M.D., 2018. CCEIII: persistent functional relationships between copepod egg production rates and food concentration through anomalously warm conditions in the California Current Ecosystem. Deep Sea Res I. 140, 26–35.
Ohman, M.D., Powell, J.R., Picheral, M., Jensen, D.W., 2012. Mesozooplankton and particulate matter responses to a deep-water frontal system in the southern California Current System. J. Plankton Res. 34 (9), 815–827.
Ohman, M.D., et al., 2013. Ecological transitions in a coastal upwelling ecosystem. Oceanography 26 (3), 210–219.
Owens, S.A., 2013. Advances in Measurements of Particle Cycling and Fluxes in the Ocean.
Owens, S.A., Buesseler, K.O., Sims, K.W.W., 2011. Re-evaluating the ^{238}U-salinity relationship in seawater: implications for the ^{238}U-^{234}Th disequilibrium method. Mar. Chem. 127 (1–4), 31–39.
Owens, S.A., Pike, S., Buesseler, K.O., 2015. Thorium-234 as a tracer of particle dynamics and upper ocean export in the Atlantic Ocean. Deep-Sea Res II 116, 42–59.
Passow, U., Dunne, J., Murray, J.W., Balistrieri, L., Alldredge, A.L., 2006. Organic carbon to Th-234 ratios of marine organic matter. Mar. Chem. 100 (3–4), 323–336.
Pike, S.M., Buesseler, K.O., Andrews, J., Savoye, N., 2005. Quantification of ^{234}Th recovery in small volume sea water samples by inductively coupled plasma-mass spectrometry. J. Radioanal. Nucl. Chem. 263 (2), 355–360.
Puigcorbé, V., et al., 2017. Latitudinal distributions of particulate carbon export across the North Western Atlantic Ocean. Deep-Sea Res. I Oceanogr. Res. Pap. 129 (Supplement C), 116–130.
Quigley, M.S., Santschi, P.H., Hung, C.-C., Guo, L., Honeyman, B.D., 2002. Importance of acid polysaccharides for 234Th complexation to marine organic matter. Limnol. Oceanogr. 47 (2), 367–377.
Quiroz, N.G.A., Hung, C.C., Santschi, P.H., 2006. Binding of thorium(IV) to carboxylate, phosphate and sulfate functional groups from marine exopolymeric substances (EPS). Mar. Chem. 100 (3–4), 337–353.
Reinfelder, J.R., Fisher, N.S., 1991. The assimilation of elements ingested by marine copepods. Science 251 (4995), 794–796.
Resplandy, L., et al., 2012. How does dynamical spatial variability impact 234Th-derived estimates of organic export? Deep-Sea Res I 68, 24–45.
Rodriguez y Baena, A.M, Fowler, S.W., Warnau, M., 2008. Could krill schools significantly bias 234Th-based carbon flux models? Limnol. Oceanogr. 53 (3), 1186–1191.
Rodriguez y Baena, A.M, Metian, M., Teyssie, J.L., De Broyer, C., Warnau, M., 2006. Experimental evidence for ^{234}Th bioaccumulation in three Antarctic crustaceans: potential implications for particle flux studies. Mar. Chem. 100 (3–4), 354–365.
Santschi, P.H., et al., 2003. Control of acid polysaccharide production and 234Th and POC export fluxes by marine organisms. Geophys. Res. Lett. 30 (2).
Santschi, P.H., et al., 2006. Thorium speciation in seawater. Mar. Chem. 100 (3–4), 250–268.
Savoye, N., et al., 2006. ^{234}Th sorption and export models in the water column: a review. Mar. Chem. 100 (3–4), 234–249.
Siegel, D.A., et al., 2014. Global assessment of ocean carbon export by combining satellite obervations and food-web models. Glob. Biogeochem. Cycles 28 (3), 181–196.
Simon, M., Grossart, H.P., Schweitzer, B., Ploug, H., 2002. Microbial ecology of organic aggregates in aquatic ecosystems. Aquat. Microb. Ecol. 28 (2), 175–211.
Stewart, G., et al., 2007. Comparing POC export from 234Th/238U and 210Po/210Pb disequilibria with estimates from sediment traps in the Northwest Mediterranean. Deep-Sea Res. I Oceanogr. Res. Pap. 54 (9), 1549–1570.
Strickland, J.D., Parsons, T.R., 1972. A Practical Handbook of Seawater Analysis, 2 ed. Bulletin of the Fisheries Research Board of Canada, pp. 167.
Stukel, M.R., Biard, T., Krause, J., Ohman, M.D., 2018. Large Phaeodaria in the twilight zone: their role in the carbon cycle. Limnol. Oceanogr. 63 (6), 2579–2594.
Stukel, M.R. and Kelly, T.B., this issue. The Carbon:^{234}Thorium ratios of sinking particles in the California Current Ecosystem 2: examination of a thorium sorption, desorption, and particle transport model. Marine Chem.
Stukel, M.R., Landry, M.R., Benitez-Nelson, C.R., Goericke, R., 2011. Trophic cycling and carbon export relationships in the California Current Ecosystem. Limnol. Oceanogr. 56 (5), 1866–1878.
Stukel, M.R., Ohman, M.D., Benitez-Nelson, C.R., Landry, M.R., 2013. Contributions of mesozooplankton to vertical carbon export in a coastal upwelling system. Mar. Ecol. Prog. Ser. 491, 47–65.
Stukel, M.R., et al., 2012. Do inverse ecosystem models accurately reconstruct plankton trophic flows? Comparing two solution methods using field data from the California current. J. Mar. Syst. 91 (1), 20–33.
Stukel, M.R., et al., 2016. The biological pump in the Costa Rica Dome: an open ocean upwelling system with high new production and low export. J. Plankton Res. 38 (2), 348–365.
Stukel, M.R., et al., 2017. Mesoscale Ocean fronts enhance carbon export due to gravitational sinking and subduction. Proc. Natl. Acad. Sci. 114 (6), 1252–1257.
Takeda, S., 1998. Influence of iron availability on nutrient consumption ratio of diatoms in oceanic waters. Nature 393 (6687), 774–777.
Taylor, A.G., et al., 2012. Sharp gradients in phytoplankton community structure across a frontal zone in the California Current Ecosystem. J. Plankton Res. 34 (9), 778–789.
Van der Loeff, M.R., et al., 2006. A review of present techniques and methodological advances in analyzing Th-234 in aquatic systems. Mar. Chem. 100 (3–4), 190–212.
Volk, T., Hoffert, M.I., 1985. Ocean Carbon pumps: analysis of relative strengths and efficiencies in ocean-driven atmospheric CO2 changes. In: Sundquist, E.T., Broeker, W.S. (Eds.), The Carbon Cycle and Atmospheric CO2: Natural Variations Archean to Present. American Geophysical Union, pp. 99–110.
Waples, J.T., et al., 2006. An introduction to the application and future use of ^{234}Th in aquatic systems. Mar. Chem. 100 (3–4), 166–189.
Wold, S., Esbensen, K., Geladi, P., 1987. Principal component analysis. Chemom. Intell. Lab. Syst. 2 (1–3), 37–52.
York, D., Evensen, N.M., Martinez, M.L., Delgado, J.D., 2004. Unified equations for the slope, intercept, and standard errors of the best straight line. Am. J. Phys. 72 (3), 367–375.
Zhang, S., Xu, C., Santschi, P.H., 2008. Chemical composition and 234Th (IV) binding of extracellular polymeric substances (EPS) produced by the marine diatom Amphora sp. Mar. Chem. 112 (1–2), 81–92.